RESEARCH ARTICLE

Therapeutically Increasing MHC-I Expression Potentiates Immune Checkpoint Blockade

Shengqing Stan Gu[1,2], Wubing Zhang[1,3], Xiaoqing Wang[4], Peng Jiang[5], Nicole Traugh[1], Ziyi Li[1,3], Clifford Meyer[1,2], Blair Stewig[1], Yingtian Xie[6], Xia Bu[4], Michael P. Manos[7], Alba Font-Tello[6], Evisa Gjini[7], Ana Lako[7], Klothilda Lim[6], Jake Conway[4], Alok K. Tewari[4], Zexian Zeng[1,2], Avinash Das Sahu[1,2], Collin Tokheim[1,2], Jason L. Weirather[1,7], Jingxin Fu[1,3], Yi Zhang[1,2], Benjamin Kroger[8], Jin Hua Liang[9,10], Paloma Cejas[6], Gordon J. Freeman[4], Scott Rodig[11], Henry W. Long[6], Benjamin E. Gewurz[9,10], F. Stephen Hodi[4,7], Myles Brown[1,4,6], and X. Shirley Liu[1,2,6]

ABSTRACT Immune checkpoint blockade (ICB) therapy revolutionized cancer treatment, but many patients with impaired MHC-I expression remain refractory. Here, we combined FACS-based genome-wide CRISPR screens with a data-mining approach to identify drugs that can upregulate MHC-I without inducing PD-L1. CRISPR screening identified TRAF3, a suppressor of the NFκB pathway, as a negative regulator of MHC-I but not PD-L1. The *Traf3*-knockout gene expression signature is associated with better survival in ICB-naïve patients with cancer and better ICB response. We then screened for drugs with similar transcriptional effects as this signature and identified Second Mitochondria-derived Activator of Caspase (SMAC) mimetics. We experimentally validated that the SMAC mimetic birinapant upregulates MHC-I, sensitizes cancer cells to T cell–dependent killing, and adds to ICB efficacy. Our findings provide preclinical rationale for treating tumors expressing low MHC-I expression with SMAC mimetics to enhance sensitivity to immunotherapy. The approach used in this study can be generalized to identify other drugs that enhance immunotherapy efficacy.

SIGNIFICANCE: MHC-I loss or downregulation in cancer cells is a major mechanism of resistance to T cell–based immunotherapies. Our study reveals that birinapant may be used for patients with low baseline MHC-I to enhance ICB response. This represents promising immunotherapy opportunities given the biosafety profile of birinapant from multiple clinical trials.

---

[1]Department of Data Science, Dana-Farber Cancer Institute, Boston, Massachusetts. [2]Department of Biostatistics, Harvard T.H. Chan School of Public Health, Boston, Massachusetts. [3]School of Life Science and Technology, Tongji University, Shanghai, China. [4]Department of Medical Oncology, Dana-Farber Cancer Institute, Boston, Massachusetts. [5]Center for Cancer Research, National Cancer Institute, Bethesda, Maryland. [6]Center for Functional Cancer Epigenetics, Dana-Farber Cancer Institute, Boston, Massachusetts. [7]Center for Immuno-Oncology, Dana-Farber Cancer Institute, Boston, Massachusetts. [8]The University of Texas Southwestern Medical School, Dallas, Texas. [9]Department of Microbiology, Harvard Medical School, Boston, Massachusetts. [10]Department of Medicine, Brigham and Women's Hospital, Boston, Massachusetts. [11]Department of Pathologic Oncology, Dana-Farber Cancer Institute, Boston, Massachusetts.

Note: Supplementary data for this article are available at Cancer Discovery Online (http://cancerdiscovery.aacrjournals.org/).

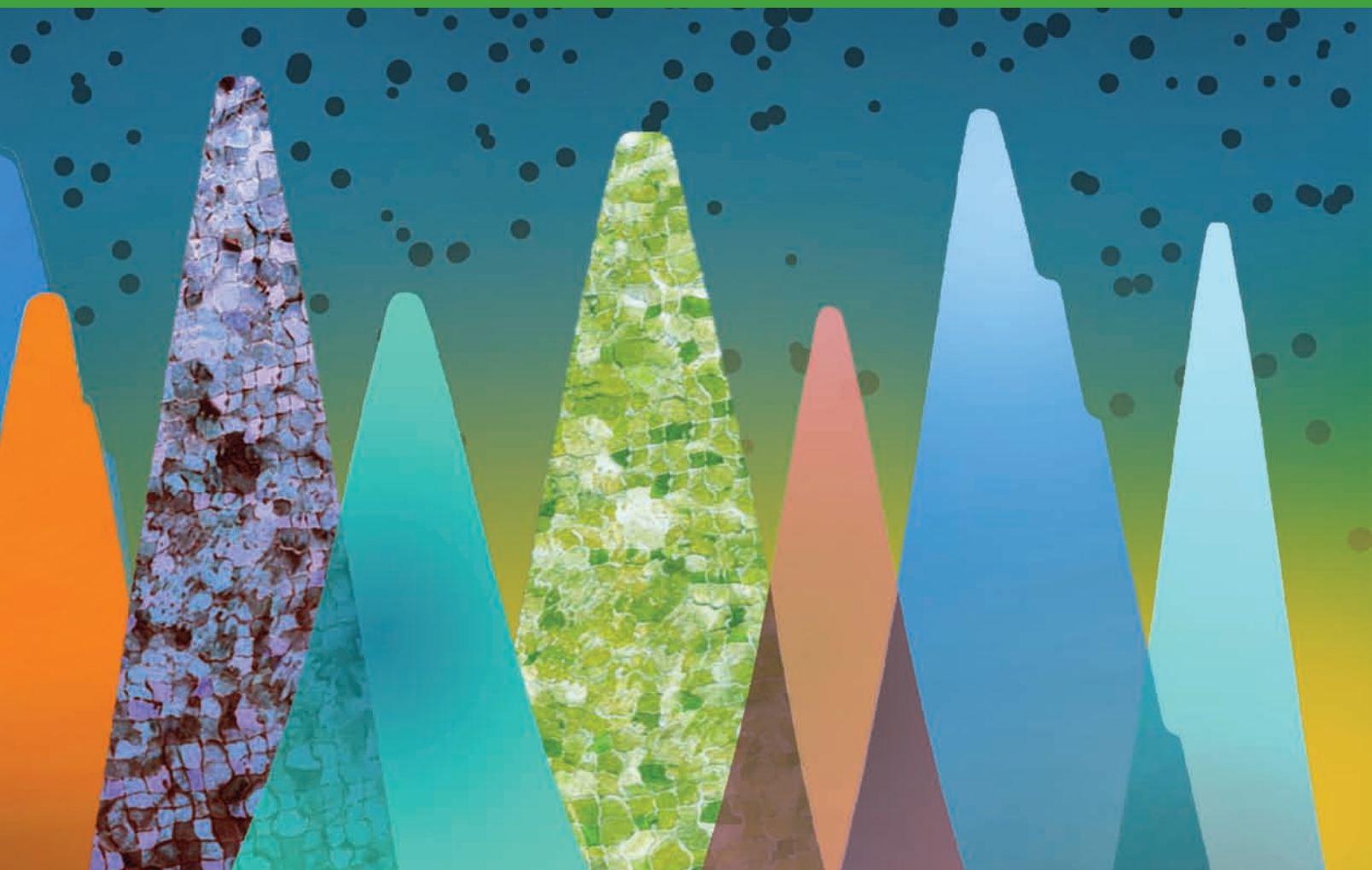S.S. Gu, W. Zhang, X. Wang, and P. Jiang contributed equally to this article.

Current address for N. Traugh: Graduate School of Biomedical Sciences, Tufts University, Boston, Massachusetts; current address for A. Font-Tello, E. Gjini, and A. Lako: Bristol Myers Squibb, Cambridge, Massachusetts.

Corresponding Authors: X. Shirley Liu, Department of Biostatistics and Computational Biology, Dana-Farber Cancer Institute, Harvard School of Public Health, 44 Binney Street, LW641, Boston, MA 02115. Phone: 617-632-2472; E-mail: xsliu@ds.dfci.harvard.edu; and Myles Brown, SM1022D, 450 Brookline Avenue, Boston, MA 02215. Phone: 617-632-3948; E-mail: myles_brown@dfci.harvard.edu

Cancer Discov 2021;11:1–18

doi: 10.1158/2159-8290.CD-20-0812

©2021 American Association for Cancer Research.

INTRODUCTION

Immune checkpoint blockade (ICB), primarily anti–PD-1, anti–PD-L1, and anti-CTLA4, has been shown to induce remarkable response across different cancer types in many clinical studies (1–8). However, only a minority of patients respond to ICB, and resistance can develop in patients who initially respond (9). The mechanisms of resistance have been under extensive investigation. Multiple cancer cell–intrinsic mechanisms have been identified, including low neoantigen load (2, 3, 10, 11), loss of antigen presentation (12, 13), loss of *HLA* heterozygosity (14, 15), impaired response or prolonged exposure to IFNγ (16–19), and activation of certain oncogenic pathways/signatures (20–22), as well as other mechanisms (22, 23). Among these ICB resistance mechanisms, insufficient antigen presentation to activate T cells comprises a large proportion of patients (24–26). MHC class I (MHC-I), the key component in antigen presentation, presents intracellular peptide antigens to the cell surface for recognition by the specific CD8^{+} T cells (27). Loss of MHC-I by genetic mutation or epigenetic silencing impairs T-cell recognition and activation, and compromises antitumor activity. Furthermore, ICB treatment of CD8^{+} T cells in the absence of antigen stimulation can induce, rather than alleviate, T-cell dysfunction (28). Therefore, enhancing MHC-I

levels in cancer cells, especially in cancers with low baseline MHC-I levels, is a promising strategy to improve ICB efficacy.

Genes encoding the MHC-I components (for example, *HLA-A/B/C* and *B2M*) are expressed widely yet are under tight regulation (29). In tumors, IFNγ secreted by tumor-infiltrating T cells can induce the expression of the MHC-I component genes through the JAK–STAT pathway (30) and boost the CD8^{+} T cell–dependent cancer cell elimination (31). However, recent reports have shown that IFNγ can also exert immunosuppressive functions, partially through its induction of immune checkpoint genes such as *CD274* (encoding PD-L1) to inhibit T-cell activation and promote T-cell dysfunction (19, 32, 33). In addition to IFNγ, multiple other cytokines were reported to upregulate both MHC-I and PD-L1 with opposite effects on tumor immunity (31). Therefore, we sought to identify gene perturbations and drugs that specifically induce MHC-I expression without increasing PD-L1 expression.

CRISPR screening is a powerful technology with increasing popularity for target identification in cancer and immunology, and FACS-based CRISPR screens have previously identified regulators of MHC-I or PD-L1 (34–36). However, it is difficult to identify factors that regulate MHC-I but not PD-L1 based on existing data, due to variations in sorting strategies and limitations in statistical power. Likewise,

several exciting studies have reported chemotherapy or targeted therapy with immunomodulatory effects by regulating MHC-I and/or PD-L1 (37–40), but a systematic approach to identifying drugs that preferentially modulate MHC-I has proved elusive.

In this study, we used a CRISPR screening approach with dual-marker FACS sorting to identify factors that decouple the regulation of MHC-I and PD-L1. The experimentally validated target was used to generate a knockout (KO) differential expression signature. Using this signature, we analyzed transcriptome data from drug perturbation studies to identify drugs that regulate MHC-I but not PD-L1. Finally, we validated the effect of the identified drug to enhance ICB response in a T cell–dependent manner *in vivo*.

RESULTS

An Integrated Workflow to Identify Drugs with MHC-I–Modulatory Effects

Analysis of bulk tumor gene expression data from The Cancer Genome Atlas (TCGA) revealed a strong positive correlation between genes encoding MHC-I and PD-L1 in multiple cancer types (Supplementary Fig. S1A). Furthermore, analysis of Cancer Cell Line Encyclopedia (CCLE) cell line gene expression data *in vitro* revealed a similar trend (Supplementary Fig. S1B). Despite the overall positive correlation, the ratio of MHC-I over PD-L1 expression is positively correlated with patient overall survival in the majority of cancer types, although TCGA tumors were not treated with immunotherapy (Supplementary Fig. S1C).

To search for drugs that can specifically upregulate MHC-I without inducing PD-L1, we designed an integrated experimental and computational workflow, which consists of five steps (Supplementary Fig. S1D). First, we performed genome-wide CRISPR screens with dual-marker sorting to identify candidate genes whose KO can upregulate MHC-I without upregulating PD-L1. Second, we performed experiments on the identified gene candidates to validate the MHC-I–specific effect and test the sensitivity to ICB therapy. Third, we characterized the target KO gene expression signature *in vitro*. Next, we searched the Gene Expression Omnibus (GEO) to identify drugs with differential gene expression signature similar to that from the candidate gene KO. Finally, we validated the drug for its immunomodulatory effects *in vitro* and *in vivo*.

CRISPR Screen Identifies TRAF3 as a Negative Regulator of MHC-I

To systematically identify regulators of MHC-I and PD-L1, we performed FACS-based genome-wide CRISPR screens using the mouse melanoma cell line B16F10 (Fig. 1A), which can be induced by IFNγ to express MHC-I and PD-L1. Low-dose (0.1 ng/mL) IFNγ showed minimal induction of MHC-I and PD-L1 and enabled us to identify negative regulators whose deficiency can increase MHC-I and/or PD-L1 protein level (Fig. 1B). In comparison, high-dose (10 ng/mL) IFNγ strongly induced MHC-I and PD-L1 and enabled us to identify the positive regulators of MHC-I and/or PD-L1 protein (Fig. 1B). We transduced the B16F10 cells with our mouse genome-wide CRISPR KO library, expanded the transduced cells, and treated the cells with either a low or high dose of IFNγ for 2 days.

We then performed FACS to isolate the MHC-I^hiPD-L1^hi, MHC-I^hiPD-L1^lo, MHC-I^loPD-L1^hi, and MHC-I^loPD-L1^lo subpopulations and compared the single guide RNA (sgRNA) frequencies in each subpopulation with the unsorted population (Fig. 1A). There was a large decrease in the number of detected sgRNAs in the regulator-enriched quadrants compared with the unsorted population, indicating strong selections in these subpopulations (Supplementary Fig. S2A).

We used the MAGeCK (refs. 41, 42; Fig. 1C; Supplementary Fig. S2B; Supplementary Table S1) and RIGER (ref. 43; Supplementary Fig. S2C) computational algorithms to analyze the CRISPR screen data. Comparison of the MHC-I^loPD-L1^lo subpopulation with the unsorted population in the 10 ng/mL IFNγ cohort identified known positive regulators of both MHC-I and PD-L1, including *Jak/Stat* and *Ifngr* genes (Fig. 1C). Comparison of the MHC-I^hiPD-L1^lo subpopulation with the unsorted population in the 10 ng/mL IFNγ cohort identified *Cd274* (encoding PD-L1), as expected, as the top PD-L1–specific positive regulator (Supplementary Fig. S2B). Comparison of the MHC-I^hiPD-L1^hi subpopulation with the unsorted population in the 0.1 ng/mL IFNγ cohort identified novel candidate common negative regulators, including *Stub1* and *Ube2n* (Fig. 1C). *Stub1* was reported to downregulate PD-L1 (35), so its role in regulating MHC-I merits further study.

The comparisons most central to the goals of this study are those differentially regulating MHC-I and PD-L1 (MHC-I^loPD-L1^hi and MHC-I^hiPD-L1^lo). Comparison of the MHC-I^loPD-L1^hi subpopulation with the unsorted population in the 10 ng/mL IFNγ condition revealed genes known to be involved in MHC-I transcription and assembly, including *B2m, Nlrc5, Tap1, Tap2, Tapbp,* and *H2-K1*, which were ranked among the top MHC-I–specific positive regulators (Fig. 1C). Comparison of the MHC-I^hiPD-L1^lo subpopulation with the unsorted population in the 0.1 ng/mL IFNγ condition identified previously reported (*Ezh2*; refs. 36, 44) and novel candidate negative regulators of MHC-I, including *Traf3, Tada3,* and *Med13* (Fig. 1C). TRAF3, the top-ranking putative MHC-I–specific negative regulator in our screens, is an adaptor protein involved in multiple signaling pathways leading to NFκB activation (45). NFκB is known to regulate MHC-I component genes by directly binding to their enhancers (46). A recent study in neuroblastoma also implicated TRAF3 as mediating the MHC-I–repressive effects of N4BP1 on MHC-I (47). These previous studies comport with our screen results that TRAF3 is a negative regulator of MHC-I.

We then validated the effect of TRAF3 perturbation on MHC-I and PD-L1 levels using CRISPR-mediated single gene KO of *Traf3* with two different sgRNAs, and overexpression of *Traf3* (Fig. 1D). As expected, *Traf3*-KO increased the expression of MHC-I, but not PD-L1, in response to various doses of IFNγ (Fig. 1E and F). Conversely, overexpression of *Traf3* specifically decreased the expression of MHC-I, but not PD-L1, in response to IFNγ (Supplementary Fig. S2D). To test whether MHC-I is upregulated by cell-extrinsic autocrines, we compared the sgControl or sg*Traf3* cells cultured in conditioned media from *Traf3*–wild-type (WT) or *Traf3*-KO cells. We did not detect a significant difference in MHC-I expression between different media conditions (Supplementary Fig. S2E). Furthermore, we compared the coculture of GFP^+ WT B16F10 cells with GFP^- *Traf3*-WT or *Traf3*-KO
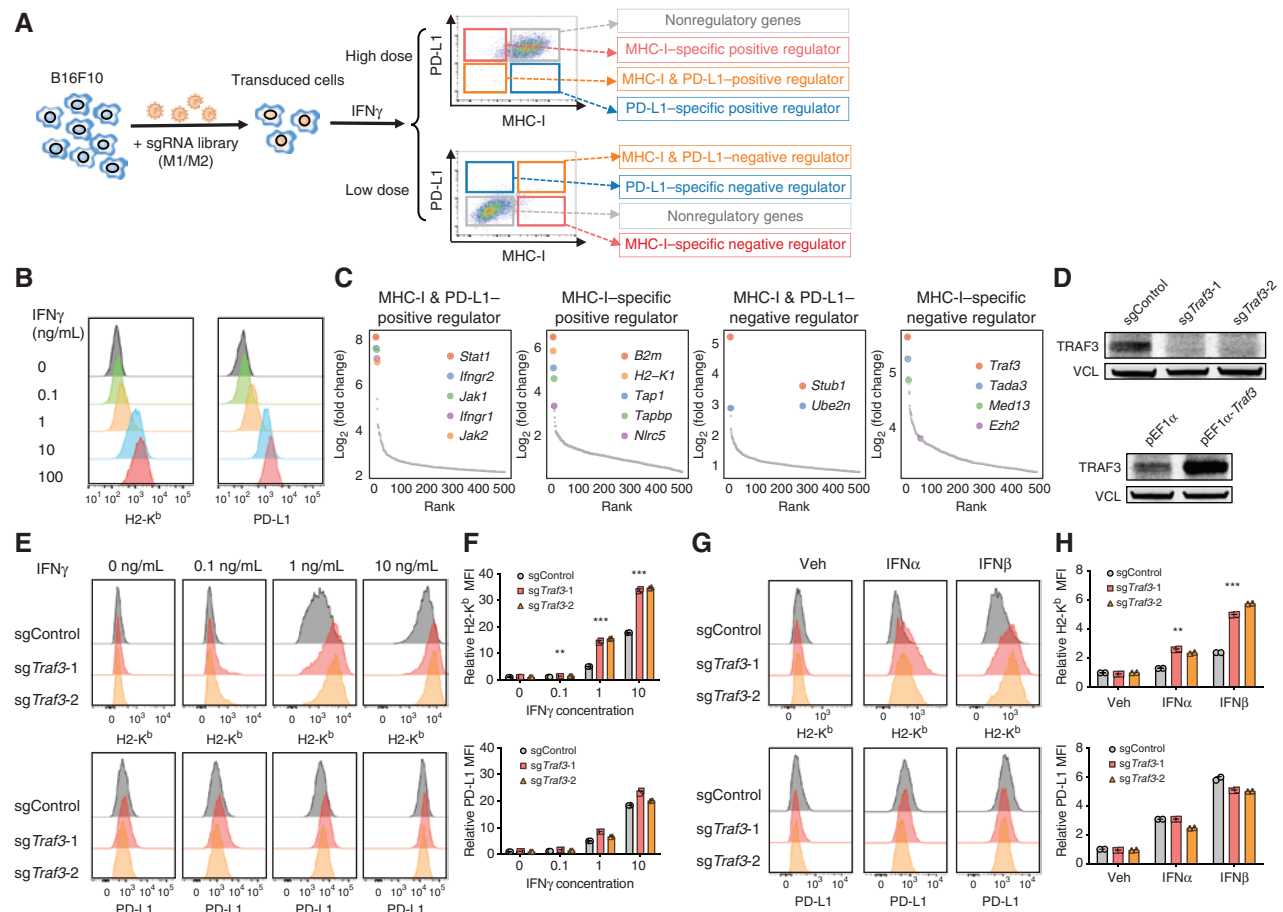
Figure 1. CRISPR screens identify novel regulators of MHC-I. **A,** Workflow of using CRISPR screens to identify the positive or negative regulators of MHC-I and/or PD-L1. We transduced B16F10 mouse melanoma cells with an in-house–designed genome-wide sgRNA library, expanded the transduced cells, and stimulated the cells with 0.1 ng/mL (low dose) or 10 ng/mL IFNγ (high dose) for different levels of MHC-I/PD-L1 induction. We then performed FACS to isolate the MHC-I^hiPD-L1^hi, MHC-I^hiPD-L1^lo, MHC-I^loPD-L1^hi, and MHC-I^loPD-L1^lo subpopulations. We amplified and sequenced the gRNAs in these subpopulations as well as the bulk presorting population to identify genes that were enriched in each sorted subpopulation. MHC-I and/or PD-L1 regulators are expected to be enriched in the subpopulations as indicated. **B,** Titration of IFNγ concentration to test its effect on MHC-I and PD-L1 expression. Histogram of H2-K^b and PD-L1 levels assessed by flow cytometry following 2-day treatment with different concentrations of IFNγ. **C,** CRISPR screen reveals known and novel candidate regulators of MHC-I and/or PD-L1. Ranked dot plots of gene enrichment in each sorted subpopulation compared with the unsorted population are shown. The X axis shows the rank of each gene, and the Y axis shows the log$_2$ enrichment of sgRNAs for each gene in the indicated subpopulation compared with the unsorted population. **D,** Immunoblot of B16F10 cells with indicated genotypes shows good efficiency of *Traf3*-KO or overexpression. **E** and **F,** Validation of TRAF3 as a negative regulator of MHC-I with IFNγ induction. B16F10 cells transduced with control sgRNA or sg*Traf3* were cultured for 48 hours, with IFNγ concentrations as indicated, and then assessed on their MHC-I and PD-L1 levels. **E,** Typical histogram of H2-K^b and PD-L1 FACS plot of control or *Traf3*-deficient B16F10 cells in each treatment condition. **F,** Quantification of median fluorescence intensity (MFI) of H2-K^b or PD-L1 from **E.** Values are normalized to the sgControl group with vehicle treatment (**, $P < 0.01$; ***, $P < 0.001$; two-way ANOVA with Benjamini–Hochberg post test comparing sg*Traf3* and sgControl in each condition). **G** and **H,** Validation of TRAF3 as a negative regulator of MHC-I with type-I IFN induction. B16F10 cells transduced with control sgRNA or sg*Traf3* were cultured for 48 hours with treatment as indicated, and then assessed on their MHC-I and PD-L1 levels. 500 U/mL IFNα or IFNβ was used. **G,** Typical histogram of H2-K^b and PD-L1 FACS plot of control or *Traf3*-deficient B16F10 cells in each treatment condition. **H,** Quantification of MFI of H2-K^b or PD-L1 from **G**. Values are normalized to the sgControl group with vehicle treatment (**, $P < 0.01$; ***, $P < 0.001$; two-way ANOVA with Benjamini–Hochberg post test comparing sg*Traf3* and sgControl in each condition).

B16F10 cells, and observed no significant difference in MHC-I expression level in GFP$^+$ WT cells between different coculture conditions either (Supplementary Fig. S2F). These data suggest that *Traf3*-KO specifically upregulates MHC-I in a cell-autonomous manner.

To test the generality of this regulation, we measured the effect of *Traf3* deficiency in the context of induction by other cytokines besides IFNγ. We found that *Traf3* deficiency also led to specific upregulation of MHC-I in response to TNFα and type I IFNs (Fig. 1G and H; Supplementary Fig. S2G and S2H). We also assessed the role of TRAF3 in MHC-I regulation in an

independent mouse cell line (Supplementary Fig. S2I–S2M), the colorectal cancer line CT26. Despite higher baseline MHC-I expression in CT26, *Traf3*-KO also led to specific upregulation of MHC-I with or without cytokine treatments (Supplementary Fig. S2I–S2M). We further tested the function of TRAF3 in human cancer cells and found that its KO can preferentially upregulate MHC-I in multiple human lines (Supplementary Fig. S2N–S2Q), including SKMEL5 (melanoma), K028 (melanoma), HT29 (colorectal cancer), and MCF7 (breast cancer). These results support the general role of TRAF3 in suppressing MHC-I in human and mouse cancer cell lines.

TRAF3 Depletion Activates MHC-I through NFκB

To study the mechanism by which TRAF3 negatively regulates MHC-I levels, we performed RNA sequencing (RNA-seq) and Assay for Transposase-Accessible Chromatin using sequencing (ATAC-seq) on *Traf3*-WT or *Traf3*-KO B16F10 cells that were treated with vehicle or 1 ng/mL IFNγ. As expected, RNA-seq revealed multiple MHC-I components, such as *H2-K1* and *H2-D1*, among the top upregulated genes in the *Traf3*-KO cells under baseline condition or after IFNγ induction (Fig. 2A; Supplementary Fig. S3A; Supplementary Table S2). Other immune-related genes were also upregulated, including the proinflammatory chemokines *Cxcl10* and *Ccl9* and components of the NFκB pathway (Fig. 2A; Supplementary Fig. S3A; Supplementary Table S2). By contrast, *Traf3*-KO did not alter the transcription of *Cd274* (PD-L1; Supplementary Table S2). Gene Ontology (GO) analysis shows that genes upregulated upon *Traf3*-KO were enriched in antigen presentation, the NFκB pathway, and TNF-mediated signaling (Fig. 2B; Supplementary Fig. S3B). This is consistent with previous reports that TRAF3 is a negative regulator of NFκB in response to various extracellular signals (48–50).

Consistent with the RNA-seq data, ATAC-seq showed that DNA accessibility is higher in *Traf3*-KO cells in the promoter regions of MHC-I components (Fig. 2C; Supplementary Fig. S3C; Supplementary Table S2). We also performed Cistrome-GO analysis (51) of the ATAC-seq data, which ranks each gene's regulatory potential with nearby peaks' strength and distance, and then examines the enrichment of GO pathways on the top-ranking genes. Genes with increased regulatory potential in *Traf3*-KO cells showed significant enrichment of antigen processing and presentation, TNF signaling pathway, and NFκB signaling pathway (Fig. 2D; Supplementary Fig. S3D). In addition, HOMER motif enrichment analysis (52) found NFκB family motif to be the most enriched in the sites with increased chromatin accessibility upon *Traf3* KO (Fig. 2E). Furthermore, we used the CistromeDB Toolkit function (53, 54) to identify transcription factors (TF) whose published binding sites have the highest overlap with our differential ATAC-seq peaks, quantified by GIGGLE score (55). This analysis found binding sites of RELA, a component of NFκB, to be the most enriched in the increased accessible sites in *Traf3*-KO cells (Fig. 2F; Supplementary Fig. S3E). Other TFs with enriched binding sites, such as AIRE, STAT3, IRF8, and STAT1 (Fig. 2F), are also known to be involved in immune response.

The NFκB pathway is involved in multiple biological processes, such as immune response, developmental processes, cell proliferation, and cell death (56–58). The NFκB family of TFs can be activated by "canonical" or "noncanonical" signaling pathways, which differ from each other in upstream regulators, TF components, and signaling kinetics (59). The canonical pathway predominantly involves RELA, cREL, and NFKB1 (p105/p50), whereas the noncanonical pathway mainly involves RELB and NFKB2 (p100/p52). Immunoblot of *Traf3*-WT or *Traf3*-KO cells with IFNγ treatment revealed that TRAF3 deficiency led to activation of both canonical pund noncanonical NFκB pathways, with increased phospho-RELA, RELB, cREL, and p52 (the active form of NFKB2; Fig. 2G and H). Analysis of existing

chromatin immunoprecipitation sequencing (ChIP-seq) datasets in Cistrome DB (53, 54) revealed that both canonical and noncanonical NFκB TFs can bind to the promoters/enhancers of MHC-I in human and mouse cells (refs. 60–62; Supplementary Fig. S3F). In addition, consistent with the reported role of TRAF3 as an adaptor for cIAP-mediated degradation of NIK (48, 49), an activator of the noncanonical NFκB pathway, TRAF3-deficient cells showed higher NIK levels (Supplementary Fig. S3G). To test whether the NFκB pathway underlies the upregulation of MHC-I in the absence of TRAF3, we treated *Traf3*-KO cells with NFκB inhibitors, TPCA-1 and IKK-16, and tested whether the upregulation of MHC-I in *Traf3*-KO cells could be reversed. Indeed, the ability of IFNγ to upregulate MHC-I was drastically attenuated when *Traf3*-KO cells were treated with TPCA-1 (Fig. 2I and J) or IKK-16 (Supplementary Fig. S3H and S3I). This finding is consistent with recent studies that activation of NFκB-related pathways can induce MHC-I expression in melanoma cells (63, 64). Taken together, these data suggest that TRAF3 deficiency leads to upregulation of MHC-I through elevated NFκB activity.

TRAF3 Deficiency Facilitates T Cell–Driven Killing of Cancer Cells

Because TRAF3 loss upregulated MHC-I but not PD-L1 in response to IFNγ, we hypothesized that it may also render cancer cells more susceptible to T cell–driven cytotoxicity. We tested this hypothesis by coculturing B16F10 cells with either Pmel-1 T cells, which have low-affinity T-cell receptors (TCR) for an endogenous melanoma antigen, or OT-I T cells, which have high affinity for an exogenously introduced ovalbumin antigen (Fig. 3A). *Traf3*-KO resulted in fewer viable cancer cells and higher MHC-I expression than *Traf3*-WT after coculture in both models (Fig. 3B–D; Supplementary Fig. S4A–S4E). In the coculture with Pmel-1 T cells, the killing efficiency in WT B16F10 cells is low at baseline due to the low expression of MHC-I. Therefore, it is common to pretreat cancer cells with IFNγ, which boosts MHC-I expression, prior to coculture with T cells in this model. We used this method and observed significantly more efficient killing of *Traf3*-KO cells (relative cell number in Fig. 3C; raw killing% in Supplementary Fig. S4C). Furthermore, we found that the *Traf3*-KO B16F10 cells could be efficiently killed by Pmel-1 T cells even without IFNγ pretreatment (relative cell number in Supplementary Fig. S4A; raw killing% in Supplementary Fig. S4D), and exhibited a substantial induction of MHC-I expression (Supplementary Fig. S4E). Conversely, overexpression of TRAF3 resulted in reduced sensitivity of cancer cells to T cell–driven cytotoxicity (relative cell number in Fig. 3E, raw killing% in Supplementary Fig. S4F).

We further tested the effect of *Traf3*-KO on tumor response to ICB treatment *in vivo*. Specifically, we transplanted *Traf3*-WT or *Traf3*-KO B16F10 cancer cells *in vivo*, treated the recipient mice with control IgG or combined anti–PD-1/anti-CTLA4 therapy, and monitored disease progression over time (Fig. 3F). Consistent with the *in vitro* coculture results, *Traf3*-KO cancer cells showed a better response to ICB treatment than *Traf3*-WT cells *in vivo*, and recipients of *Traf3*-KO cancer cells survived significantly longer upon ICB treatment (Fig. 3G and H). Interestingly, *Traf3*-KO tumors also grew
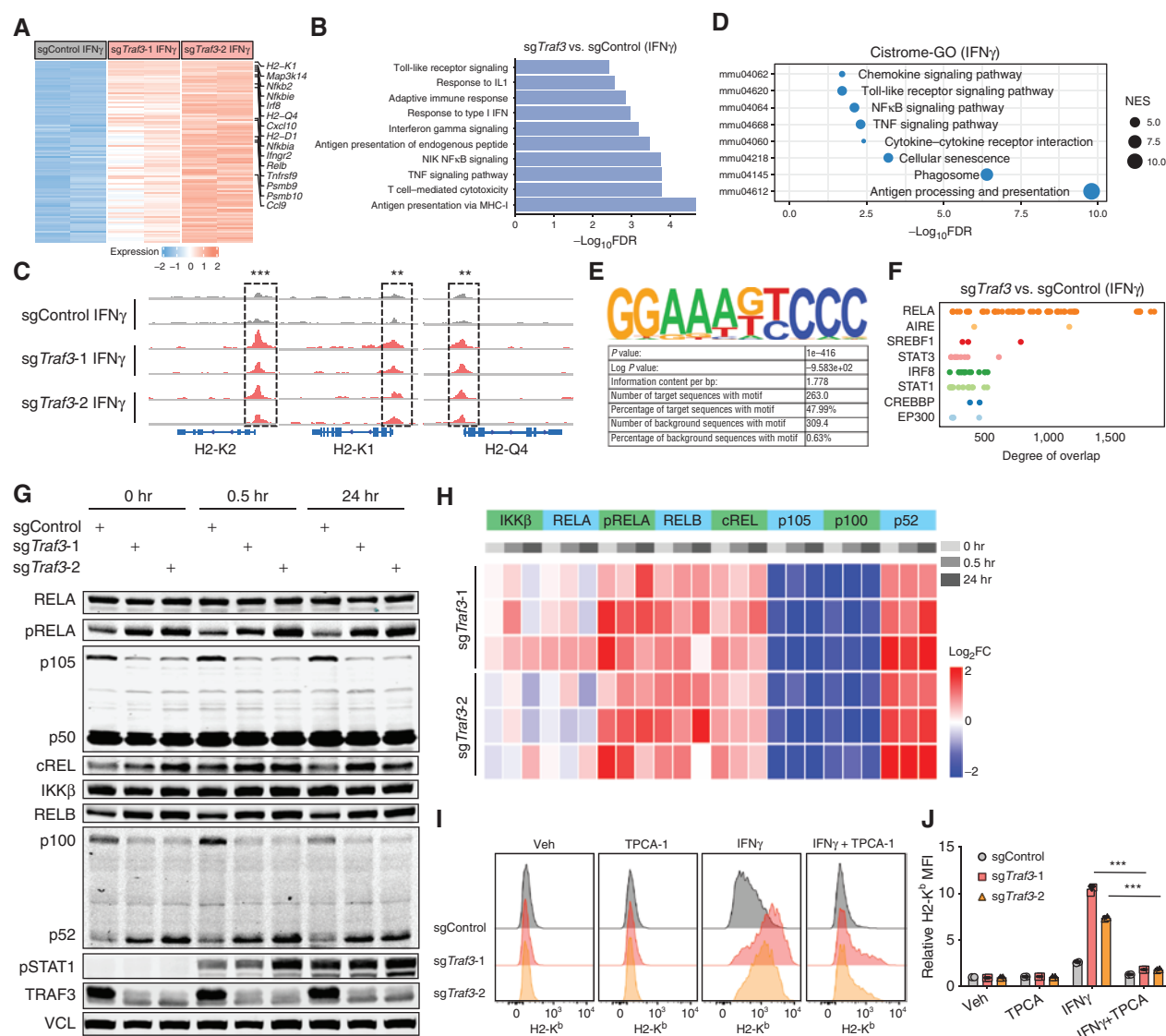
Figure 2. TRAF3 deficiency upregulates MHC-I through NFκB. **A,** RNA-seq of B16F10 cells transduced with sgControl or sg*Traf3* shows upregulation of MHC-I–related genes in the absence of *Traf3*. Heat map of differential expression of genes induced by TRAF3 deficiency with IFNγ treatment. **B,** Gene set enrichment analysis of upregulated pathways (GO biological pathway) in sg*Traf3* cells compared with sgControl cells with IFNγ treatment. Multiple pathways, such as antigen presentation and NFκB signaling, were upregulated by the deletion of *Traf3*. **C,** ATAC-seq of *Traf3*-normal or -deficient B16F10 cells revealed that TRAF3 deficiency leads to higher chromatin accessibility near genes encoding components of the MHC-I complex. **, $P < 0.01$; ***, $P < 0.001$. **D,** Cistrome-GO analysis of the more accessible regions in sg*Traf3* compared with sgControl cells with IFNγ treatment. **E,** Cistrome toolkit analysis of ATAC-seq data revealed that DNA-binding sites of RELA were more open in the *Traf3*-deficient cells. **F,** Enrichment of motifs in the accessible chromatin regions specific to *Traf3*-deficient cells. The top enriched motifs (RELA) are shown. **G,** Typical immunoblot of NFκB signaling components in *Traf3*-normal or *Traf3*-deficient B16F10 cells in response to IFNγ induction. B16F10 cells transduced with sgControl or sg*Traf3* were induced by 1 ng/mL IFNγ for 0, 0.5, or 24 hours, and then harvested for immunoblot. Data from one typical experiment out of three biological replicates is shown. **H,** Quantification of immunoblot signals from **G** based on three biological replicates. TRAF3 deletion leads to upregulated NFκB signaling. **I** and **J,** B16F10 cells transduced with control sgRNA or sg*Traf3* were treated with vehicle control, IFNγ (1 ng/mL), and/or TPCA-1 (1 μmol/L) for 48 hours, and then assessed on their MHC-I and PD-L1 levels. **I,** Typical histogram of H2-K^b and PD-L1 FACS plot of control- or *Traf3*-deficient B16F10 cells in each treatment condition. **J,** Quantification of MFI of H2-K^b or PD-L1 from **I**. Values are normalized to sgControl group with vehicle treatment (***, $P < 0.001$; two-way ANOVA with Benjamini–Hochberg post test comparing IFNγ and IFNγ+TPCA groups).

more slowly than TRAF3-normal tumors even without ICB (Fig. 3G). In addition, depletion of CD8 T cells by anti-CD8 treatment ablated the slower tumor growth caused by *Traf3*-KO, with control IgG or ICB treatment (Supplementary Fig. S4G). This indicated that the effect of *Traf3*-KO on tumor growth is dependent on the presence of CD8 T cells.

To provide further support of our experimental observations, we analyzed multiple published coculture or *in vivo* CRISPR screens. In general, *Traf3*-KO tended to sensitize cancer cells to T cell–driven cytotoxicity in those studies (Supplementary Fig. S4H), in agreement with our finding. In contrast, in natural killer (NK)–cell coculture CRISPR screens, *Traf3*-KO
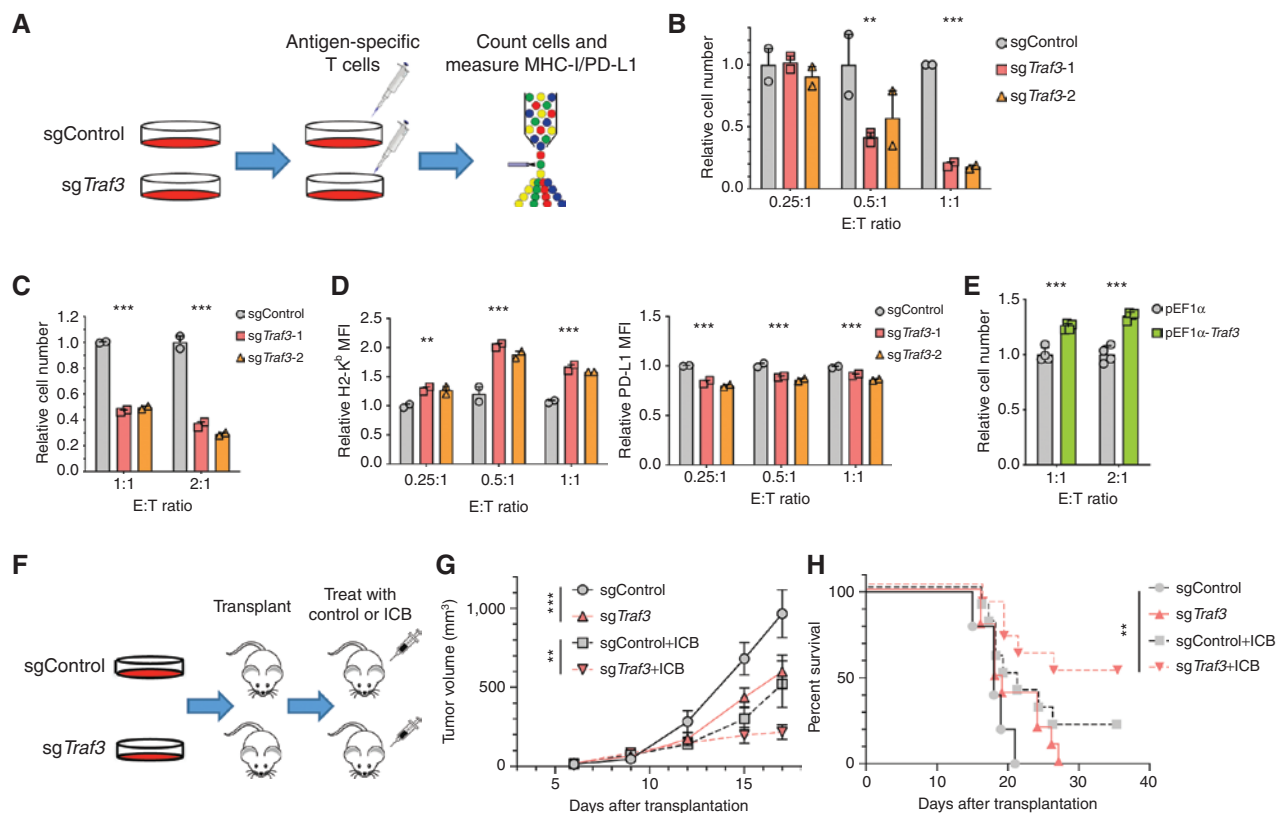
Figure 3. TRAF3 deletion sensitizes cancer cells to T cell–driven cytotoxicity. **A,** Workflow of testing the role of TRAF3 in regulating the response of cancer cells to T cell–driven cytotoxicity through *in vitro* coculture. *Traf3*-normal or *Traf3*-deficient B16F10 cells were cultured with antigen-specific CD8+ T cells (Pmel-1 or OT-I) for 1 to 3 days. Cell number and cell surface MHC-I/PD-L1 expression were quantified by FACS. **B** and **C,** Relative B16F10 cell number after coculture with (**B**) OT-I T cells or (**C**) Pmel-1 T cells at different Effector:Target (E:T) ratios revealed a higher sensitivity of *Traf3*-deficient B16F10 cells to T-cell–mediated cytotoxicity. For coculture with Pmel-1 T cells, B16F10 cells were pretreated with 1 ng/mL IFNγ for 12 hours prior to the coculture. The bar plots present the relative cell number in each group, normalized to the cell number in the sgControl group in each E:T condition. Mean ± SD and individual replicate values are shown for each group (**, $P < 0.01$; ***, $P < 0.001$; two-way ANOVA with Benjamini–Hochberg post test comparing sg*Traf3* and sgControl in each condition). **D,** Relative MFI of H2-K^b or PD-L1 of B16F10 cells cocultured with OT-I T cells. Values are normalized to the sgControl group in E:T = 0.25 condition. Mean ± SD and individual replicate values are shown for each group (**, $P < 0.01$; ***, $P < 0.001$; two-way ANOVA with Benjamini–Hochberg post test comparing sg*Traf3* and sgControl in each condition). **E,** Relative B16F10 cell number after coculture with Pmel-1 T cells at different E:T ratios revealed a lower sensitivity of *Traf3*-overexpressing B16F10 cells to T cell–mediated cytotoxicity. The bar plots present the relative cell number in each group, normalized to the cell number in the pEF1α group in each E:T condition. Mean ± SD and individual replicate values are shown for each group (**, $P < 0.01$; ***, $P < 0.001$; two-way ANOVA with Benjamini–Hochberg post test comparing pEF1α-*Traf3* and pEF1α in each condition). **F,** Workflow of testing the role of TRAF3 in modulating the ICB response *in vivo*. 4×10^5 B16F10 cells (*Traf3*-normal or *Traf3*-deficient) were transplanted subcutaneously into syngeneic recipient mice. Starting on day 6 after transplantation, we treated the recipients with control IgG or combination ICB every third day for a total of four doses. We monitored tumor size and recipient survival. **G,** Longitudinal tumor size of sgControl or sg*Traf3* tumors treated by control IgG or ICB. Mean ± SEM is shown for each group at each time point (**, $P < 0.01$; ***, $P < 0.001$; two-way ANOVA with Benjamini–Hochberg post test comparing sg*Traf3* and sgControl in each condition). **H,** Kaplan–Meier curves of recipients of sgControl or sg*Traf3* tumors treated by control IgG or ICB. The sg*Traf3* cohort with ICB treatment survived significantly longer than the other groups (**, $P < 0.01$; log-rank test with Benjamini–Hochberg adjustment of multiple comparisons).

seemed to desensitize cancer cells to NK-cell killing (Supplementary Fig. S4I), consistent with the role of MHC-I in inhibiting NK-cell cytotoxicity (65).

Traf3-KO Signature Is Correlated with Higher MHC-I in Primary Patient Samples

Next, we evaluated whether TRAF3 function was correlated with MHC-I expression or T-cell infiltration in clinical cohorts where bulk tumor RNA-seq has been performed. Because TRAF3 regulates downstream TF activity, rather than directly using *TRAF3* expression itself to measure TRAF3 functional deficiency, we derived a *Traf3*-KO gene expression signature from RNA-seq (Supplementary Fig. S5A; Supple-

mentary Table S3). Specifically, we used the top differential genes from TRAF3 deficiency as signature genes, and evaluated the *Traf3*-KO signature score in each clinical tumor RNA-seq sample by a weighted sum of signature gene expression. We further used it to assess the association of TRAF3 deficiency with MHC-I antigen presentation, cytotoxic T-cell infiltration, overall survival, and immunotherapy response in clinical cohorts as appropriate.

We first examined TCGA tumors, where baseline antitumor immunity can influence prognosis, although patients were not treated with ICB (66, 67). We found the *Traf3*-KO signature level to be positively correlated with MHC-I expression, CD8+ T-cell infiltration, and patient survival in melanoma
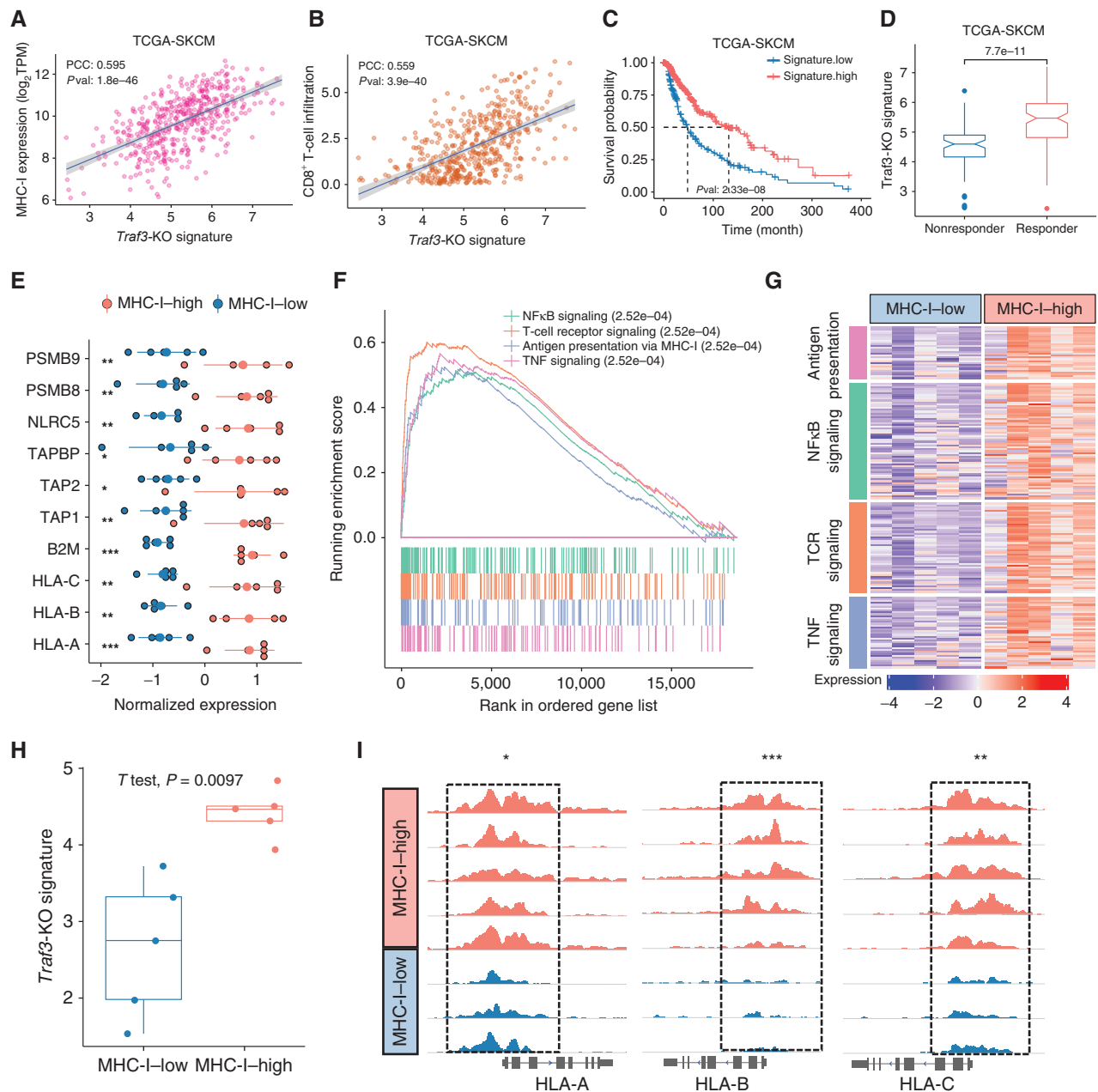
Figure 4. *Traf3*-KO signature is correlated with higher MHC-I in primary patient samples. **A–C,** *Traf3*-KO signature is positively correlated with (**A**) MHC-I expression, (**B**) CD8+ T-cell infiltration, and (**C**) patient survival in the TCGA-SKCM dataset. PCC, Pearson correlation coefficient; TPM, Transcripts Per Kilobase Million. **D,** TIDE-predicted ICB responders showed higher *Traf3*-KO signature values in the TCGA SKCM (skin cutaneous melanoma) dataset. **E,** Expression of MHC-I component or related genes in MHC-I–high or MHC-I–low samples. **F,** Gene set enrichment analysis of differentially expressed genes in MHC-I–high versus MHC-I–low samples. **G,** MHC-I–high samples show higher expression of genes involved in antigen presentation, NFκB signaling, TNF signaling, and Toll-like receptor pathways. **H,** *Traf3*-KO signature score in MHC-I–high or MHC-I–low RNA-seq samples. **I,** H3K27ac ChIP-seq results for the *HLA-A/B/C* loci in MHC-I–high or MHC-I–low samples. (*continued on next page*)

(Fig. 4A–C). We also applied an orthogonal algorithm TIDE (66), which we developed to predict ICB response based on expression signatures of T-cell dysfunction and exclusion, to TCGA tumors as if they were to be treated with ICB. The predicted responders also showed higher *Traf3*-KO signature score than the predicted nonresponders (Fig. 4D). Furthermore, we observed positive correlation of *Traf3*-KO signature

and MHC-I expression, CD8 T-cell infiltration, and patient survival in multiple other cancer types in TCGA (Supplementary Fig. S6A–S6D). Finally, to assess the MHC-I–specific effect of *Traf3*-KO, we created a restricted *Traf3*-KO signature to include just the differential genes in the MHC-I component genes. This MHC-I–restricted *Traf3*-KO signature still shows positive correlation with patient survival in many
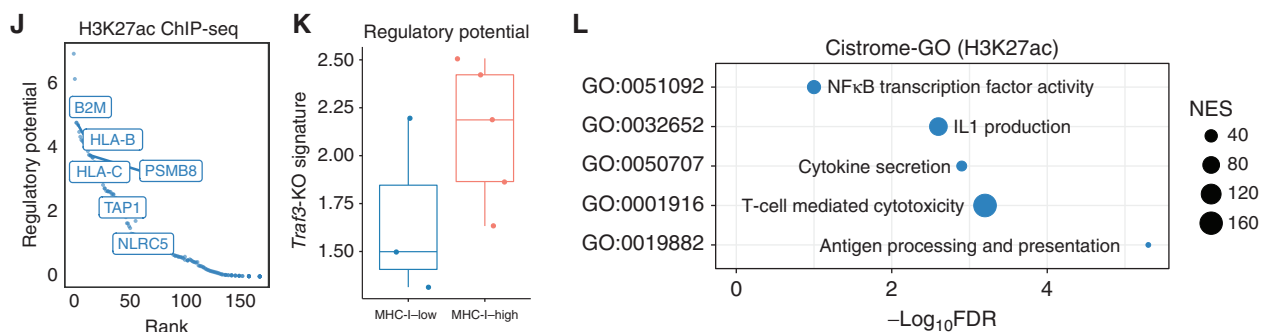
Figure 4. *(Continued)* **J,** Top 200 genes with the higher regulatory potential value in MHC-I–high versus MHC-I–low H3K27ac ChIP-seq samples. **K,** *Traf3*-KO signature score of H3-K27ac ChIP-seq regulatory potential values in MHC-I–high or MHC-I–low samples. **L,** Cistrome-GO enrichment analysis of H3K27ac ChIP-seq peaks with stronger signal in MHC-I–high compared with MHC-I–low samples. *, $P < 0.05$; **, $P < 0.01$; ***, $P < 0.001$.

cancer types in TCGA (Supplementary Fig. S6E). These results suggest that the MHC-I–induction effect by TRAF3 inhibition is associated with better clinical outcome.

In addition to publicly available databases, we also collected primary samples from treatment-naïve patients with melanoma treated at the Dana-Farber Cancer Institute. Assessment of MHC-I levels by immunohistochemistry (IHC) of the formalin-fixed paraffin-embedded (FFPE) samples identified MHC-I–high and MHC-I–low tumors, from which we macrodissected cancer cell sections for RNA-seq and H3K27 acetylation fixed tissue ChIP-seq (FitAc-seq; ref. 68) to examine the molecular features associated with MHC-I expression. RNA-seq results on MHC-I components (*HLA-A, HLA-B, HLA-C*, and *B2M*) and other genes in the same pathway were consistent with the IHC results (Fig. 4E). Examination of the differentially expressed genes revealed 673 upregulated and 425 downregulated genes in the MHC-I–high compared with the MHC-I–low samples, with the upregulated genes being enriched in NFκB and TNF signaling pathways (Fig. 4F and G; Supplementary Table S4). Indeed, MHC-I–high samples showed a significantly higher *Traf3*-KO signature score (Fig. 4H). Consistent with the RNA-seq data, ChIP-seq revealed higher levels of H3K27ac near MHC-I and higher regulatory potential of MHC-I–related genes (Fig. 4I and J; Supplementary Table S4). The regulatory potential of *Traf3*-KO signature genes was also higher in the MHC-I–high samples (Fig. 4K). Cistrome GO analysis of the differentially active chromosomal regions from ChIP-seq revealed that NFκB binding sites are more active in the MHC-I–high samples (Fig. 4L). These results suggest that the negative regulation of MHC-I by TRAF3 is also reflected in the primary melanoma tumors from patients.

Traf3-KO Signature Is Correlated with Better ICB Response

In patients treated with immunotherapy, antigen expression and/or presentation levels are known to be a critical factor of treatment response and an issue addressed in multiple response biomarker studies (12, 69). Higher MHC-I expression is associated with better ICB response in most published ICB cohorts (Supplementary Fig. S7A). Based on the role of TRAF3 in MHC-I regulation, we tested the correlation between TRAF3 functional deficiency and immunotherapy

response in the published ICB treatment cohorts. We examined the RNA-seq data of pretreatment biopsies in a recent melanoma cohort with 63 biopsies treated with anti–PD-1 monotherapy and 57 treated with combined anti–PD-1 and anti-CTLA4 (70). We confirmed that the *Traf3*-KO signature was positively correlated with tumor MHC-I, cytotoxic T-cell infiltration, ICB response, and progression-free survival (Fig. 5A–D). Because the MHC-I–TCR interaction is a conserved mechanism for T-cell recognition of cancer cells, we expect the *Traf3*-KO signature to be associated with ICB response in various cancer types.

We therefore applied our findings to another study with approximately 300 urothelial carcinoma biopsies (71), the largest published cohort with available expression data. Again, *Traf3*-KO signature was positively correlated with tumor MHC-I, cytotoxic T-cell infiltration, ICB response, and progression-free survival (Fig. 5E–H). Furthermore, the complete or MHC-I–restricted *Traf3*-KO signature showed a similar trend (Supplementary Table S5; Fig. 5I; Supplementary Fig. S7B–S7E) in most published ICB clinical studies across different cancer types. Together, our data support the general relevance of *Traf3*-KO signature in predicting ICB response.

Identification of a SMAC Mimetic, Birinapant, as a Regulator of MHC-I to Enhance ICB Efficacy

Based on the effect of *Traf3*-KO on MHC-I levels and sensitivity to T cell–driven killing, we hypothesized that drug treatment that mimics the transcriptional effect of *Traf3*-KO may achieve similar outcomes. We searched existing transcriptomic studies on drug-treatment effects in the GEO database, with differential expression data involving more than 200 targeted therapy/chemotherapy drugs. Different drug treatments showed distinct transcriptional regulation of MHC-I components and PD-L1/PD-L2 (Fig. 6A; Supplementary Fig. S8A; Supplementary Table S6). We computed the *Traf3*-KO signature score of each drug treatment, and, reassuringly, it is significantly positively correlated with MHC-I expression (Supplementary Fig. S8B). Focusing on drugs that increase *Traf3*-KO signature and MHC-I expression, we found several drugs previously reported to upregulate MHC-I, including the CDK4/6 inhibitor palbociclib (38) and the EZH2 inhibitor
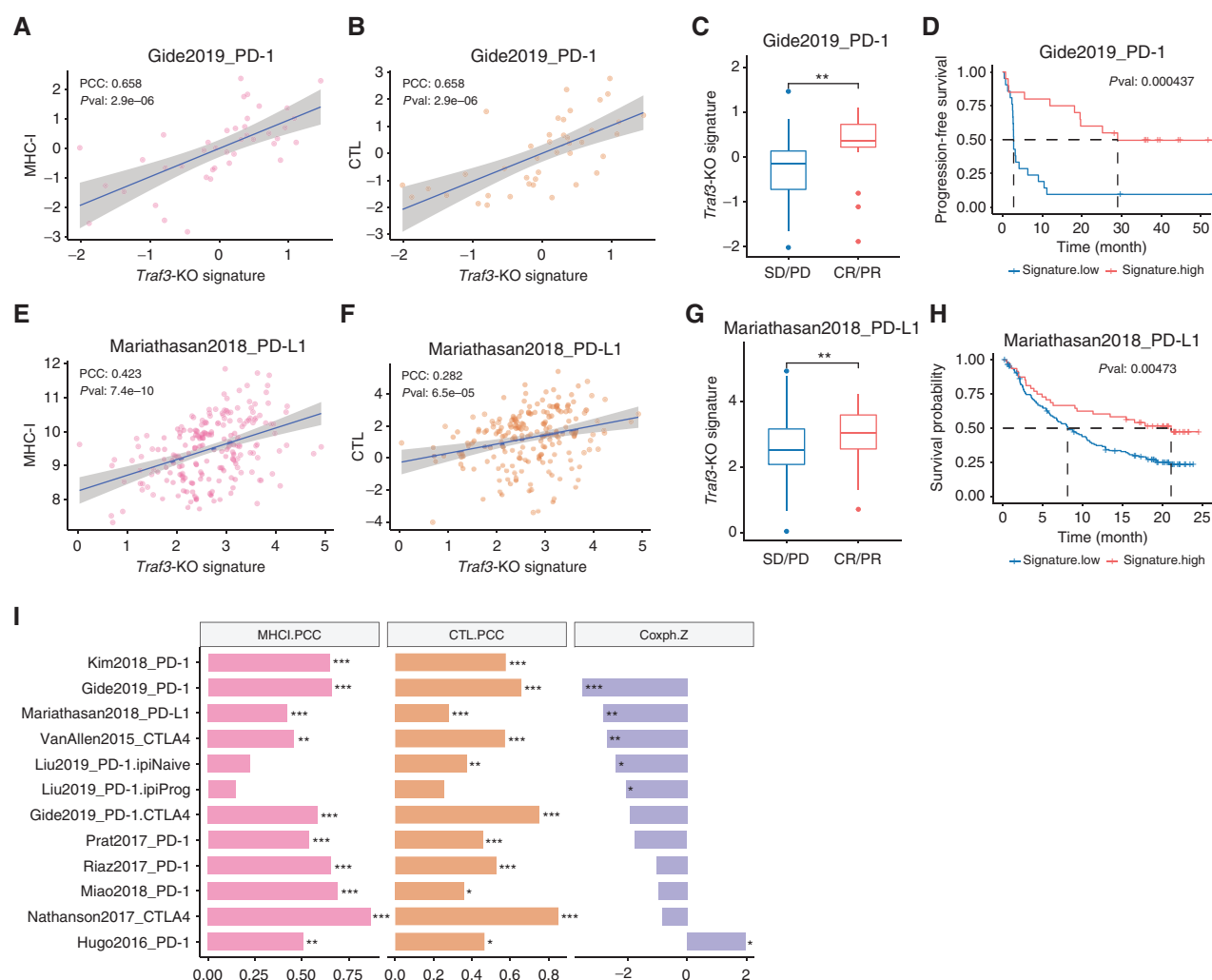
Figure 5. *Traf3*-KO signature is correlated with better response to ICB. **A–D,** *Traf3*-KO signature is positively correlated with (**A**) MHC-I expression, (**B**) intratumoral cytotoxic T lymphocyte (CTL) infiltration, (**C**) ICB response, and (**D**) overall survival and progression-free survival in patients treated by anti–PD-1 or combined anti–PD-1 and anti-CTLA4 in the Gide and colleagues (70) study in melanoma. **E–H,** *Traf3*-KO signature is positively correlated with (**E**) MHC-I expression, (**F**) intratumoral CTL infiltration, (**G**) ICB response, and (**H**) overall survival and progression-free survival in patients treated by anti–PD-1 or combined anti–PD-1 and anti-CTLA4 in the Mariathasan and colleagues (71) study in urothelial carcinoma. **I,** *Traf3*-KO signature is positively correlated with MHC-I expression and cytotoxic T-cell infiltration and negatively correlated with survival hazard in most ICB treatment clinical trials. *, $P < 0.05$; **, $P < 0.01$; ***, $P < 0.001$. PD, progressive disease; SD, stable disease; PR, partial response; CR, complete response.

EPZ6438 (ref. 44; Supplementary Table S6). Furthermore, we found multiple Second Mitochondria-derived Activator of Caspase (SMAC) mimetics as novel candidates for MHC-I–specific regulation (Fig. 6B). SMAC mimetics are a family of proapoptotic compounds that can inhibit the cIAP/XIAP E3 ligases, leading to activated NFκB activity. We therefore examined the immunomodulatory effects of a SMAC mimetic, birinapant, using *in vitro* and *in vivo* assays.

We first tested the effect of birinapant treatment on MHC-I levels in mouse B16F10 and CT26 cells. Indeed, birinapant treatment specifically upregulated MHC-I in response to IFNγ treatment, with minimal effect on PD-L1 (Fig. 6C and D; Supplementary Fig. S8C). Furthermore, birinapant can also specifically upregulate MHC-I in multiple human cancer cell lines (Supplementary Fig. S8D–S8G). Similar to the effect of *Traf3*-KO, birinapant treatment led to reduced inactive

forms of NFκB (p100 and p105) and increased active form of NFκB (p52; Supplementary Fig. S8H). Consistent with the reported role of SMAC mimetics to induce cIAP degradation (72, 73), we found lower cIAP and higher NIK levels in birinapant-treated cells (Supplementary Fig. S8I). When added to the cancer cells cocultured with OT-I T cells, birinapant resulted in specific upregulation of MHC-I in cancer cells and facilitated better cancer cell killing by T cells (Fig. 6E and F). We further tested whether this immunomodulatory effect of birinapant functions through TRAF3 in cancer cells by using *Traf3*-WT or *Traf3*-KO cancer cells cocultured with antigen-specific T cells, treated by vehicle or birinapant. TRAF3-deficient cancer cells showed comparable high levels of MHC-I expression and sensitivity to T cell–mediated cytotoxicity as birinapant-treated cells, and were not further sensitized by birinapant (Supplementary Fig. S8J and S8K).
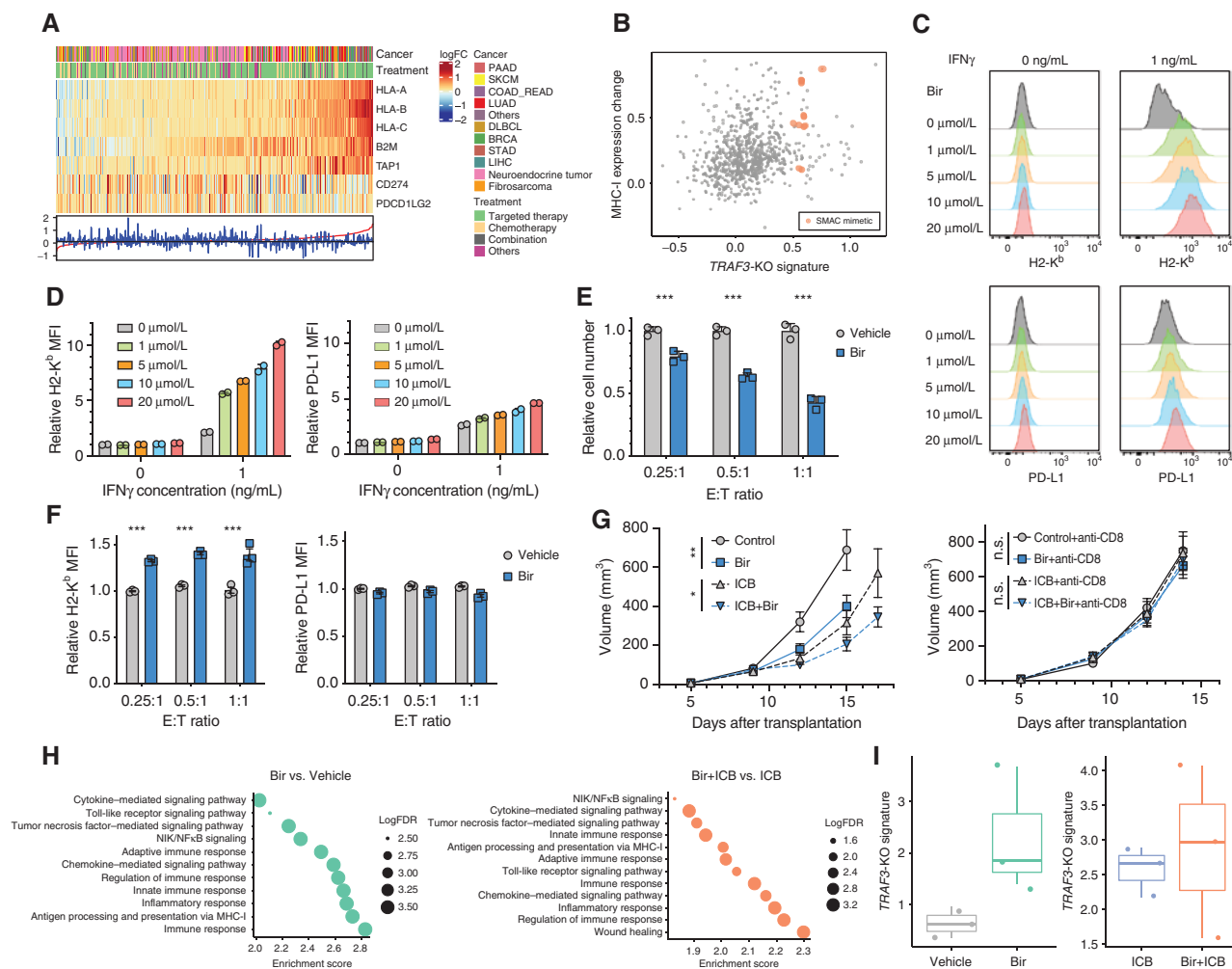
Figure 6. Birinapant can specifically upregulate MHC-I and add to the efficacy of ICB treatment. **A,** Heat map of the regulation of transcription of MHC-I components and PD-L1/PD-L2 in each drug treatment condition. Data are ordered by the magnitude of MHC-I regulation from the most upregulated (left) to the most downregulated (right). **B,** Characterization of each drug treatment for effect on MHC-I expression and *Traf3*-KO signature value. **C,** Flow cytometry of B16F10 cells treated by IFNγ and/or different concentrations of the SMAC mimetic birinapant (Bir). Typical histograms of H2-K[b] and PD-L1 levels in each condition are shown. **D,** The relative MFI of samples in **C**. Mean ± SD is shown for each group. Values are normalized to the mean MFI at 0 ng/mL IFNγ and 0 μmol/L birinapant. **E,** Relative B16F10 cell number after coculture with OT-I T cells at different E:T ratios revealed a higher sensitivity of B16F10 cells to T cell–mediated cytotoxicity under birinapant treatment. The bar plots present the relative cell number in each group, normalized to the cell number in the vehicle treatment group in each E:T condition. Mean ± SD and individual replicate values are shown for each group (***, $P < 0.001$; two-way ANOVA with Benjamini–Hochberg post test). **F,** Relative MFI of H2-K[b] or PD-L1 of B16F10 cells cocultured with OT-I T cells. Values are normalized to the vehicle treatment group in E:T = 0.25 condition. Mean ± SD and individual replicate values are shown for each group (***, $P < 0.001$; two-way ANOVA with Benjamini–Hochberg post test comparing vehicle and SMAC treatment groups in each condition). **G,** Longitudinal tumor size of tumors under different treatments. Mean ± SEM is shown for each group at each time point (*, $P < 0.05$; **, $P < 0.01$; two-way ANOVA with Benjamini–Hochberg post test). **H,** Gene set enrichment analysis of the bulk tumor RNA-seq data evaluating the gene sets that were upregulated in response to SMAC mimetic. **I,** Quantification of *Traf3*-KO signature in each treatment group revealed a trend toward upregulation in response to birinapant treatment.

These data suggest that birinapant's effect on MHC-I expression is dependent on the presence of TRAF3.

We further tested the effect of birinapant *in vivo* by treating established B16F10 melanoma tumors with birinapant and/or combination anti–PD-1/CTLA4. We observed moderately reduced tumor growth *in vivo* with birinapant treatment alone, and further reduced tumor progression with combination therapy of birinapant and ICB (Fig. 6G, left). In addition, CD8 T-cell depletion by anti-CD8 treatment ablated the slower tumor growth caused by birinapant treatment (Fig. 6G, right), indicating the effect of birinapant treatment

on tumor growth to be CD8 T-cell–dependent. We performed RNA-seq of the bulk tumor in each treatment group to identify the pathways regulated by birinapant. Indeed, birinapant-upregulated genes, whether with ICB treatment or not, are involved in inflammatory response, innate/adaptive immune response, chemokine/cytokine-mediated signaling, NFκB signaling, and MHC-I antigen presentation (Fig. 6H; Supplementary Table S7). Inference of tumor immune infiltration by TIMER (74, 75) predicted a trend for higher infiltration of dendritic cells and CD8+ T cells, though the difference is not statistically significant (Supplementary Fig. S8L and S8M).

In addition, birinapant treatment increased the *Traf3*-KO signature in the tumor (Fig. 6I, left), consistent with our *in silico* prediction and *in vitro* epistatic experiment showing that SMAC mimetic treatment phenocopies *Traf3*-KO. In contrast, we did not observe a significant difference in *Traf3*-KO signature between birinapant + ICB and ICB groups (Fig. 6I, right). Because we evaluated tumor RNA-seq after ICB treatment, the cancer cells that show higher *Traf3*-KO signature were likely more susceptible to immune killing, making it difficult to detect such signature through bulk tumor RNA-seq. This ICB-induced selection for immune-resistant clones was characterized in our recent work applying clonal tracing of cancer cells following ICB treatment (76). Furthermore, the presence of other cell types in the tumor microenvironment might obscure the enrichment of *Traf3*-KO signature.

DISCUSSION

Immunotherapy, especially ICB, has brought paradigm shifts to cancer treatment and improved patient survival in many cancer types. Its therapeutic effect relies on the recognition of cancer-specific antigens by cytotoxic T cells, and defect in cancer cell antigen presentation is a major ICB-resistance mechanism. Multiple studies have sought to identify regulators of MHC-I (36, 44). However, due to the common regulatory pathways shared by MHC-I and PD-L1, upregulating MHC-I often leads to upregulation of PD-L1, which suppresses antitumor immunity. In this study, we established a workflow to identify drugs with MHC-I–specific enhancing effects. We first performed dual-marker FACS-based CRISPR screens to identify regulators of MHC-I and/ or PD-L1, and found TRAF3 as an MHC-I–specific negative regulator through its modulation of the NFκB pathway. TRAF3 depletion sensitized cancer cells to antigen-specific T cell–driven cytotoxicity. *Traf3*-KO signature is significantly correlated with higher expression of genes in the antigen presentation pathway, higher cytotoxic T-cell infiltration, and better overall survival in patients with cancer from many TCGA cohorts and ICB clinical trials. Furthermore, data mining of public transcriptomic profiles of drug treatment followed by experimental validation identified that birinapant, a SMAC mimetic, phenocopies the effect of TRAF3 deficiency on MHC-I expression and adds to the efficacy of ICB treatment in suppressing tumor growth. Our study identifies a novel treatment strategy that can potentially be used in MHC-I–low cancers to enhance ICB therapeutic efficacy.

TRAF3 has been reported to negatively regulate the NFκB pathway activity, and multiple ChIP-seq studies revealed NFκB binding sites in the promoter/enhancer regions of MHC-I components. Consistent with these previous studies, we found that *Traf3*-KO upregulates MHC-I in an NFκB-dependent manner. There are no published TRAF3 small-molecule inhibitors, so we searched published studies to identify drugs that phenocopy the effect of TRAF3 inhibition. The SMAC mimetic family ranked among the top of the list. SMAC mimetics can trigger the autoubiquitination and degradation of Cellular Inhibitor of Apoptosis Proteins (cIAP), thereby promoting NFκB activation via canonical or noncanonical pathways (49, 77). We then experimentally validated that birinapant, a SMAC mimetic, can promote the immu-

nosensitivity of cancer cells through specifically inducing MHC-I expression in a TRAF3/NFκB-dependent manner. A recent study also showed that SMAC mimetics can synergize with ICB in a CD8 T cell–dependent and TNFα-dependent manner (78), although SMAC mimetics did not upregulate MHC-I in their glioblastoma model (CT-2A). Our preliminary analyses of published single cell RNA-seq (scRNA-seq) data from various cancer types (79) found that glioblastoma cells tend to have high expression of MHC-I and NFκB component genes. We speculate that cells already high in MHC-I and NFκB might not increase MHC-I when treated with SMAC mimetics. Indeed, in A375 and 786O cell lines with higher baseline MHC-I and NFκB expression, birinapant also failed to increase MHC-I. These results suggest context-dependent MHC-I regulation and antitumor response induced by SMAC mimetics, which merit further mechanistic studies.

In addition to SMAC mimetics, mining the GEO database identified multiple other targeted therapy or chemotherapy agents with the potential to cause a transcriptional effect similar to TRAF3 inhibition. This comports with multiple other studies (37–39, 80, 81) in revealing the immunomodulatory effects of chemotherapy and targeted therapies. For example, palbociclib, a CDK4/6 inhibitor reported to induce MHC-I via type-III IFN (38), and EPZ6438, an EZH2 inhibitor reported to induce MHC-I via chromatin modification (36, 44), ranked among the top candidates. Regimens containing azacitidine, another top-ranking candidate, were also reported to induce antigen presentation in non–small cell lung cancer cells (82). Our approach using differential gene expression signatures can be extended to identify drugs with other immunomodulatory effects.

Our study has limitations that future studies could address. First, our finding can potentially assist the treatment of tumors whose MHC-I is suppressed through gene regulatory mechanisms, but not those with genetic deletion of MHC-I components or loss of heterozygosity of *HLA* genes. Nevertheless, the clinical observation in melanoma treated by ICB (13) suggests that a large number of patients can still benefit from this approach. Second, in addition to upregulation of MHC-I, other mechanisms may also contribute to the immune sensitivity of *Traf3*-KO tumors. For example, *Traf3*-KO cells had higher expression of chemokines which may facilitate T-cell infiltration. Further studies are needed to elucidate such alternative mechanisms and their impact on the immune sensitivity of *Traf3*-KO tumors. Third, when mining drug treatment data to predict drugs that may upregulate MHC-I through TRAF3/NFκB, our analysis may be limited by the amount of drug treatment data available in GEO. More publicly available transcriptional profiling data on drug screening would improve the power of our approach.

In summary, we present a workflow integrating CRISPR screens with functional genomics characterization and computational mining of publicly accessible data to identify novel regulators of tumor immunity. We showed that the SMAC mimetic birinapant can phenocopy TRAF3 deficiency and preferentially induce MHC-I expression, leading to enhanced sensitivity of cancer cells to T cell–driven cytotoxicity. The combination of SMAC mimetic and ICB is likely to benefit patients with a low baseline level of MHC-I expression. This is potentially exciting given the biosafety of profiles of birinapant from multiple early-phase clinical studies. Furthermore,

our general approach can be applied to identify other drugs with immunomodulatory effects.

METHODS

TCGA Cohorts

We downloaded all the TCGA tumor data from the Broad GDAC Firehose, including transcriptomic profiles and clinical information of tumor samples, from 33 cancer types. All of the gene expression levels were measured by logarithmic Transcripts Per Kilobase Million (TPM). We downloaded the IHC-derived tumor purity data from the study by Aran and colleagues (83), and we also estimated the tumor purity using the CHAT algorithm (84). For all the tumors, we estimated the immune cell infiltration in the tumor microenvironment using TIMER algorithm, with default parameters and TPM as input. Because of the distinct clinical behavior and molecular profile of cancer subtypes, we divided breast cancer datasets into the PAM50 subtypes of basal, lumA, lumB, and HER2 positive. We focused on cancer types where higher MHC-I is associated with better overall survival (CoxPH regression of patient survival proportional hazard and MHC-I expression with a z-score < –0.5) for downstream analyses.

CCLE Cohorts

We downloaded the RNA-seq data of more than 1,000 cancer cell lines from the DepMap Portal, which contains processed gene expression data quantified according to the Genotype-Tissue Expression pipelines.

Flow Cytometry

We performed FACS of B16F10 or CT26 cells treated under different conditions as indicated to quantify the level of H2-K^b/H2-K^d and PD-L1. B16F10 or CT26 cells were dissociated by TrypLE treatment, washed with PBS-2% FBS, and incubated with DAPI (1:10,000 dilution), anti–H2-K^b (clone AF6-88.5, BioLegend, 1:400 dilution), and anti–PD-L1 (clone MIH5, BD Biosciences, 1:400 dilution) for 1 hour on ice. Cells were then washed and resuspended in PBS-2% FBS and analyzed on BD LSR-Fortessa instrument. FACS data were then analyzed by Flowjo software.

Cell Lines and Cell Culture

Cell lines B16F10, CT26, SKMEL5, and MCF7 were purchased from the ATCC and authenticated using standard short tandem repeat analysis in 2019. Cell line K028 was derived from a patient with melanoma under Institutional Review Board–approved protocols. Cell line HT29 was obtained from the CCLE core facility, which obtained them directly from commercial sources and authenticated the lines using standard short tandem repeat analysis. 293FT, B16F10, SKMEL5, K029, and MCF7 were cultured in DMEM supplemented with 10% FBS, 1% L-glutamine, and 1% penicillin and streptomycin. CT26 and HT29 were cultured in RPMI supplemented with 10% FBS, 1% L-glutamine, and 1% penicillin and streptomycin. All cells were used at low passage numbers and were tested for *Mycoplasma* using the MycoAlert Mycoplasma Detection Kit (Lonza).

CRISPR Screens for Regulators of MHC-I

We performed CRISPR screens to identify regulators of MHC-I induced by IFNγ. We first transduced 1×10^8 B16F10 cells with our M1/M2 mouse genome-wide CRISPR library at multiplicity of infection of 0.3 to ensure that most transduced cells received only 1 virion. We cultured the transduced cells for 2 days in DMEM full media, selected with 2 μg/mL puromycin for 2 days, and cultured for an additional 2 days to allow depletion of residual protein of the targeted genes. We then treated the cells with high- or low-dosage IFNγ to identify MHC-I regulators.

For identification of positive regulators, we treated the transduced cells with 10 ng/mL IFNγ for 2 days and flow-sorted 2×10^7 cells for the following populations: MHC-I^{hi} PD-L1^{hi}, MHC-I^{hi} PD-L1^{lo}, MHC-I^{lo} PD-L1^{hi}, MHC-I^{lo} PD-L1^{lo}. The sgRNAs that are present in the MHC-I^{lo} PD-L1^{hi} population are expected to enrich for MHC-I–specific positive regulators. For identification of negative regulators, we treated the transduced cells with 0.1 ng/mL IFNγ for 2 days, and flow-sorted 2×10^7 cells for the following populations: MHC-I^{hi} PD-L1^{hi}, MHC-I^{hi} PD-L1^{lo}, MHC-I^{lo} PD-L1^{hi}, MHC-I^{lo} PD-L1^{lo}. The gRNAs that are present in the MHC-I^{hi} PD-L1^{lo} population are expected to enrich for MHC-I–specific negative regulators.

Genomic DNA extraction and gRNA library construction were performed as described before (85). Briefly, we extracted genomic DNA from each sorted population or from the unsorted population by phenol–chloroform extraction, and then performed two rounds of PCR to construct the barcode-indexed sequencing library for each sample. We sequenced each library at an approximately 300× average coverage over the CRISPR library.

Analysis of CRISPR Screen

MAGeCK software was used to quantify and test for sgRNA and gene enrichment (41). The sequence reads were trimmed to remove a constant portion of the sgRNA sequences and mapped to the M1/M2 mouse genome-wide CRISPR library with MAGeCK "count" module, which computes read counts for each sgRNA. We used MAGeCK "test" module to identify MHC-I/PD-L1 regulators, for which targeting sgRNA was significantly enriched in the sorted populations compared with the control unsorted populations grown in parallel. MAGeCK returned sgRNA and gene log fold changes, which represent the enrichment level of the sgRNAs and genes in each cell population. Because negative selection is meaningless in FACS-based CRISPR screens, we assigned zero log fold change for genes whose log fold changes were negative. Finally, we calculated the mean log fold change of genes in M1 and M2 CRISPR screens and visualized the results using functions in R package MAGeCKFlute (42).

We analyzed the data from the cohort treated by 10 ng/mL IFNγ to identify the positive regulators of MHC-I and/or PD-L1. Specifically, we compared the gRNA distribution between the MHC-I^{lo} PD-L1^{lo} population and unsorted population to identify positive regulators for both; between the MHC-I^{lo} PD-L1^{hi} population and the unsorted population to identify MHC-I–specific positive regulators; and between the MHC-I^{hi} PD-L1^{lo} population and the unsorted population to identify PD-L1–specific positive regulators.

We analyzed the data from the cohort treated by 0.1 ng/mL IFNγ to identify the negative regulators of MHC-I and/or PD-L1. Specifically, we compared the gRNA distribution between the MHC-I^{hi} PD-L1^{hi} population and unsorted population to identify negative regulators for both; between the MHC-I^{hi} PD-L1^{lo} population and the unsorted population to identify MHC-I–specific negative regulators; and between the MHC-I^{lo} PD-L1^{hi} population and the unsorted population to identify PD-L1–specific negative regulators.

Cloning of Screen Candidates for Validation

We cloned four gRNAs of *Traf3* into the LentiCRISPRv2-Puro construct to validate the role of TRAF3 in the regulation of MHC-I. We used the cloning protocol as previously established (86, 87). Out of the four gRNAs, two successfully depleted TRAF3 protein level >80%. We used these two gRNAs for our follow-up validation studies.

We also cloned the open reading frame of *Traf3* into pER1α-Puro vector for overexpression of *Traf3* and examination of its role in MHC-I/PD-L1 regulation.

Validation of the Role of TRAF3 in MHC-I/PD-L1 Regulation

We performed CRISPR/Cas9–mediated deletion of *Traf3* in multiple cell lines, including B16F10 and CT26. For each line, we cultured

Traf3-normal or *Traf3*-deficient cells with different dosages of IFNγ, TNFα, IFNα, or IFNβ for 2 days to test its regulation of MHC-I and/or PD-L1 with these induction methods.

Virus Packaging

Viral packaging was performed as previously described (85). Briefly, we cultured 293FT cells at 40% to 50% confluence the day before transfection. Transfection was performed using X-tremeGENE HD (Sigma-Aldrich). For each 10-cm dish, 8 µg of lentivectors, 2.4 µg of pMD2.G, and 6 µg of psPAX2 were added into 2 mL Opti-MEM (Life Technologies). Forty microliters of X-tremeGENE HD was added to the plasmid mixture. The complete mixture was incubated for 15 minutes and then added to 1.1×10^7 293FT cells per 10-cm dish. After overnight culture, the media were changed to 8 mL DMEM + 15% FBS for virus collection. We harvested virus at 48, 60, and 72 hours after the start of transfection.

Coculture of Cancer Cells and T Cells for T-cell Cytotoxicity Assay

Coculture of cancer cells and T cells was performed as previously described (66). Briefly, B16F10 cells were maintained in complete DMEM (10% FBS and 50 U/mL of penicillin–streptomycin). CD8 T cells isolated from spleen and lymph nodes from Pmel-1 or OT-I mice were stimulated with anti-CD3/CD28 beads (Thermo Fisher, 11452-D) and then cultured in complete RPMI 1640 media (10% FBS, 20 mmol/L HEPES, 1 mmol/L sodium pyruvate, 0.05 mmol/L 2-mercaptoethanol, 2 mmol/L L-glutamine, 50 U/mL streptomycin and penicillin, and 20 ng/mL recombinant mouse IL2).

To test the sensitivity of cancer cells to T cell–driven cytotoxicity (OT-I or Pmel-1 model), we plated B16F10 cells (sg*Rosa26*, sg*Traf3*, pEF1a-Empty, or pEF1a-*Traf3*) at equal density in all wells and added T cells at ratios to cancer cells. With the OT-I model, we first incubated the B16F10 cells with 1 nmol/L SIINFEKL peptide for 2 hours prior to coculture with T cells. With the Pmel-1 model, B16F10 cells were either pretreated with 1 ng/mL IFNγ overnight or untreated prior to the coculture. There are two to four cell-culture replicates for each condition. After a 1-day or 3-day coculture with T cells, we counted the remaining cancer cells by FACS using the precision count beads (BioLegend, 424902). T cells present in these cultures were gated out based on antibodies specific for CD45 (BioLegend, clone 30-F11) or CD8 (BioLegend, clone 53-6.7).

Immunoblot

We treated B16F10 cells (sg*Rosa26* or sg*Traf3*) by 1 ng/mL IFNγ for 0, 0.5, or 24 hours and lysed cells in RIPA buffer. Lysates were resolved by SDS-PAGE, and immunoblotting was performed as described (88). To visualize NIK levels, cells were pretreated by 0 or 5 µmol/L MG132 for 4 hours before lysis. Antibodies specific for TRAF3, STAT1, phospho-STAT1(Y705), RELA, RELB, phospho-RELA(S536), cREL, p100/p52, p105/p50, IKK, and NIK were from Cell Signaling Technology. Antibody specific for VCL was from Santa Cruz Biotechnology. Antibody specific for cIAP was from R&D Systems. Antibodies were used at each manufacturer's recommended concentrations.

RNA-seq

For comparison of transcription profile between control and *Traf3*$^{-/-}$ B16F10 cells, we treated sgControl or sg*Traf3*-transduced B16F10 cells with vehicle control or 1 ng/mL IFNγ for 2 days, and extracted total RNA using the miRNeasy Plus Mini Kit (QIAGEN, #17004) following the manufacturer's protocol. For comparison of tumors treated by birinapant and/or ICB, we harvested bulk tumors from recipients in each group on day 15 after transplantation and extracted total RNA. Total RNA samples in each experiment were submitted to Novogene Inc. for sequencing. Standard mRNA library

preparation kit was used for library preparation. Paired-end 150 bp sequencing was performed on Illumina HiSeq 2500. Sequencing reads were mapped to the mm10 genome by RSEM. Statistics for differentially expressed genes were calculated by DESeq2.

Traf3-KO Signature

To study the clinical relevance of TRAF3, we established a *Traf3*-KO signature by extracting the top 200 upregulated and 200 downregulated genes and taking the normalized DESeq2 Wald statistics as weights. The weights of genes are normalized to –1 to 1 range by the equation $k_i = w_i/max(w)$, where k_i indicates the weight of the *i*th gene, and w_i indicates the DESeq2 Wald statistics of the *i*th gene. For each input expression profile, we computed a *Traf3*-KO signature score to estimate the *Traf3*-KO level by calculating the weighted sum expression of the signature genes following the equation $S = \sum_{i=1}^{n}(k_i * X_i)$, where S denotes the signature score, and X_i denotes the expression level of the *i*th gene. Finally, we evaluated the association of TRAF3 deficiency with MHC-I expression, tumor-infiltrating T cells, patient outcome, and response to ICB.

ATAC-seq

For comparison of chromatin accessibility between control and *Traf3*$^{-/-}$ B16F10 cells, we treated sgControl or sg*Traf3*-transduced B16F10 cells with vehicle control or 1 ng/mL IFNγ for 2 days. ATAC-seq was performed in duplicates (200,000 cells) by the Center for Functional Cancer Epigenetics at Dana-Farber Cancer Institute as previously described (76, 89). For data analysis, we used Burrows–Wheeler Aligner (90) to map sequencing reads to the reference genome and MACS2 (91) for peak calling. DESeq2 (92) was applied to identify the differentially accessible regions between ICB-resistant lines and the parental control line.

Mouse Experiments

All mice were housed in standard cage in Dana-Farber Cancer Institute Animal Resources Facility (ARF). All animal procedures were carried out under the ARF Institutional Animal Care and Use Committee (IACUC) protocol and were in accordance with the IACUC standards for the welfare of animals. WT C57BL/6 recipient mice were purchased from Charles River laboratory.

To test the function of TRAF3 in tumor's response to combination anti–PD-1/anti-CTLA4 treatment, we transplanted 4×10^5 sg*Rosa26* or sg*Traf3* B16F10 cells subcutaneously into the right flank of 6- to 8-week-old female C57BL/6 mice (from Charles River Laboratory). Starting day 6 after transplantation, we began treatment with control IgG [clone 2A3, 200 µg per mouse in 200 µL Hank's Balanced Salt Solution (HBSS) buffer] or combination anti–PD-1 (clone 1A12, 100 µg per mouse) and anti-CTLA4 (clone 9D9, 100 µg per mouse) by i.p. injection every third day for a total of 4 times. We monitored tumor growth along the treatment.

To test the efficacy of ICB and SMAC mimetic combination treatment, we transplanted 4×10^5 parental B16F10 cells subcutaneously into the left and right flanks of 6- to 8-week-old female C57BL/6 mice (from Charles River Laboratory). Starting day 5 after transplantation, we began treatment with vehicle or birinapant (dissolved in 15% captisol, 600 µg per mouse) by i.p. injection every third day for a total of 3 times. Starting day 6 after transplantation, we began treatment with control IgG (clone 2A3, 200 µg per mouse in 200 µL HBSS buffer) or combination anti–PD-1 (clone 1A12, 100 µg per mouse) and anti-CTLA4 (clone 9D9, 100 µg per mouse) by i.p. injection every third day for a total of 3 times. We monitored tumor growth along the treatment and the survival of recipients.

Mice were euthanized using CO_2 inhalation. All mouse experiments were performed in compliance with institutional guidelines as approved by the IACUC of Dana-Farber Cancer Institute. The

maximum tumor diameter permitted under the relevant animal protocols is 20 mm, which was not exceeded in any experiment.

Profiling of Primary MHC-I–High or MHC-I–Low Melanoma Samples

For comparison of transcription and epigenetic profile between MHC-I–high and MHC-I–low primary melanoma tumors, we performed RNA-seq and FiTAc-seq of human tumor biopsies. Samples were grouped into MHC-I–high or MHC-I–low based on IHC of tumor biopsy from the same sampling.

FiTAc-seq: H3K27Ac ChIP-seq on FFPE Samples

FiTAc-seq (68) was used to profile H3K27ac ChIP-seq on FFPE samples. Sample selection was performed with dual-IHC staining assessing tumor enrichment with SOX10 antibody and MHC-I expression status. Accordingly, areas of interest were marked, and samples were classified into low or high MHC-I categories. The selected areas of interest were manually macrodissected from 10 unstained sections (10 µmol/L each) per case. Briefly, the macrodissected tissues were washed with xylenes to remove paraffin, rehydrated in an ethanol/water series, and incubated overnight with 200 µL of lysis buffer [1% SDS, 50 mmol/L Tris-HCl (pH 8), and 10 mmol/L EDTA] on a thermomixer set at 65°C and shaking at 1,000 rpm. Next, samples were put on ice, supplemented with protease and deacetylase inhibitors, and sonicated with Covaris E220 instrument for 5 minutes (PIP105, 5% DF, 200 cbp) in 1 mL AFA Fiber milliTUBEs. Solubilized chromatin (ranging from 450 ng to 3 µg) was precleared, diluted, and immunoprecipitated overnight with 3 µg of H3K27ac antibody (Diagenode, cat. #A1723-0041-D, lot #C15410196) following a low-input protocol; and finally washed, eluted, and DNA purified. Libraries were prepared with the Accel-NGS 2S Plus DNA Library Kit (Swift Biosciences, cat. no. 21024) on an automated next-generation sequencing (NGS) workstation, amplified for 14 cycles, and sequenced on a Next-seq instrument (PE35).

Immunotherapy Trials

We collected 12 cancer patient cohorts with available RNA-seq data, patient survival, and immunotherapy response from published studies, including more than 900 ICB-treated tumors from 61 gastric cancer, 420 melanoma, 35 renal cell carcinoma, and 348 urothelial cancer. For each cohort, we standardized the transcriptome data across patients by variance stabilizing transformation.

Drug Treatment Transcriptomic Data

By searching for transcriptomic studies on drug perturbation from GEO, we manually collected 719 expression profiles, including both microarray and RNA-seq datasets. Microarray profiles were normalized by the normalizeQuantiles function in limma. For each dataset, we then performed differential expression analysis with limma (for microarray) or DESeq2 (for RNA-seq). Finally, for each drug treatment condition, we got the pattern of gene expression change, which served as the input gene expression signature into signature-based analysis for mining immune-modulating drugs.

Testing the Effect of SMAC Mimetic Birinapant on MHC-I Expression and Sensitivity to T Cell–Driven Killing

To test the effect of birinapant on MHC-I and PD-L1 expression, we treated B16F10 or CT26 cells with IFNγ (0 or 1 ng/mL) and/or birinapant (0, 1, 5, 10, or 20 µmol/L) for 48 hours and tested the effects on MHC-I or PD-L1 expression by flow cytometry.

To test the effect of birinapant on sensitivity of cancer cells to T cell–driven cytotoxicity, we started treatment of B16F10 cells (parental, sgRosa26, or sgTraf3) with vehicle control or 1 µmol/L birinapant 24 hours prior to the coculture and maintained the same condition throughout the coculture.

Testing the combination efficacy of SMAC mimetic and ICB *in vivo* is detailed in the section "Mouse Experiments" above.

Correlation Analysis

We took the average $\log_2$TPM of HLA-A, HLA-B, HLA-C, and B2M as MHC-I expression, and then tested the correlation between MHC-I and PD-L1 expression by using Pearson's correlation adjusted by tumor purity estimated by IHC or the CHAT algorithm (83) in 25 cancer types in TCGA. MHC-I and PD-L1 show strong positive correlation in the majority of cancer types, where they also show strong correlation with CD8 T-cell infiltration. We also computed the correlation between MHC-I and PD-L1 expression in cancer cell lines, which shows the similar results.

We calculated the Pearson correlation of TRAF3-KO signature score with MHC-I expression and CTL level (average expression of CD8A, CD8B, GZMA, GZMB, and PRF1) in multiple tumor cohorts. The TRAF3-KO signature score shows notable positive correlation with MHC-I expression and CTL level in most of the TCGA cancer types and immunotherapy trials.

Survival Analysis

We used the Cox proportional hazards regression analysis to test the association between MHC-I expression and patient survival and selected 16 cancer types, in which the MHC-I expression is positively correlated with patient survival (coxph z-statistics < –0.5), for downstream analysis. To determine the decoupled effect of MHC-I and PD-L1 on patient survival, we tested the association between MHC-I/PD-L1 differential expression and patient survival, and found patients with higher MHC-I/PD-L1 differential expression have longer overall survival in all the 16 cancer types.

The clinical relevance of TRAF3 regulating MHC-I expression is confirmed by testing the association between TRAF3-KO signature and overall survival or progressive survival of patients in TCGA and immunotherapy trials with cox regression.

Gene Set Enrichment/Overrepresentation Analysis

All pathway/GO enrichment analyses were performed using the EnrichAnalyze function in MAGeCKFlute R package, and the enriched pathways are visualized using functions from MAGeCKFlute.

Cistrome-GO and Toolkit for CistromeDB Analysis

We selected top 1,000 enriched peaks from ATAC-seq or H3K27ac ChIP-seq and entered the BED file into Cistrome-GO website to perform pathway enrichment analysis and Toolkit to identify the TFs that have a significant binding overlap with the input peak sets.

Data Availability

All sequencing data were uploaded to GEO with accession number GSE149826.

Code Availability

All codes are available upon request.

Authors' Disclosures

Authors' Contributions

S.S. Gu: Conceptualization, formal analysis, validation, investigation, methodology, writing–original draft, writing–review and editing. **W. Zhang:** Conceptualization, data curation, formal analysis, investigation, methodology, writing–original draft, writing–review and editing. **X. Wang:** Formal analysis, validation, investigation, methodology, writing–review and editing. **P. Jiang:** Conceptualization, formal analysis, investigation, methodology, writing–review and editing. **N. Traugh:** Formal analysis, validation, investigation. **Z. Li:** Formal analysis, validation, investigation. **C. Meyer:** Conceptualization, methodology. **B. Stewig:** Validation, investigation. **Y. Xie:** Formal analysis. **X. Bu:** Investigation. **M.P. Manos:** Investigation. **A. Font-Tello:** Investigation. **E. Gjini:** Investigation. **A. Lako:** Investigation. **K. Lim:** Investigation. **J. Conway:** Investigation. **A.K. Tewari:** Investigation. **Z. Zeng:** Investigation. **A. Das Sahu:** Investigation. **C. Tokheim:** Investigation. **J.L. Weirather:** Investigation. **J. Fu:** Investigation. **Y. Zhang:** Investigation. **B. Kroger:** Validation, investigation. **J.H. Liang:** Investigation. **P. Cejas:** Investigation. **G.J. Freeman:** Supervision, writing–review and editing. **S. Rodig:** Resources, investigation. **H.W. Long:** Resources, investigation. **B.E. Gewurz:** Supervision, investigation, writing–review and editing. **F.S. Hodi:** Resources, supervision, investigation. **M. Brown:** Conceptualization, resources, supervision, writing–review and editing. **X.S. Liu:** Conceptualization, resources, supervision, writing–review and editing.

Acknowledgments

REFERENCES

1. Topalian SL, Hodi FS, Brahmer JR, Gettinger SN, Smith DC, McDermott DF, et al. Safety, activity, and immune correlates of anti-PD-1 antibody in cancer. N Engl J Med 2012;366:2443–54.
2. Snyder A, Makarov V, Merghoub T, Yuan J, Zaretsky JM, Desrichard A, et al. Genetic basis for clinical response to CTLA-4 blockade in melanoma. N Engl J Med 2014;371:2189–99.
3. Le DT, Uram JN, Wang H, Bartlett BR, Kemberling H, Eyring AD, et al. PD-1 blockade in tumors with mismatch-repair deficiency. N Engl J Med 2015;372:2509–20.
4. Hodi FS, O'Day SJ, McDermott DF, Weber RW, Sosman JA, Haanen JB, et al. Improved survival with ipilimumab in patients with metastatic melanoma. N Engl J Med 2010;363:711–23.
5. Ansell SM, Lesokhin AM, Borrello I, Halwani A, Scott EC, Gutierrez M, et al. PD-1 blockade with nivolumab in relapsed or refractory Hodgkin's lymphoma. N Engl J Med 2015;372:311–9.
6. Powles T, Eder JP, Fine GD, Braiteh FS, Loriot Y, Cruz C, et al. MPDL3280A (anti-PD-L1) treatment leads to clinical activity in metastatic bladder cancer. Nature 2014;515:558–62.
7. Ferris RL, Blumenschein G Jr, Fayette J, Guigay J, Colevas AD, Licitra L, et al. Nivolumab for recurrent squamous-cell carcinoma of the head and neck. N Engl J Med 2016;375:1856–67.
8. McDermott DF, Sosman JA, Sznol M, Massard C, Gordon MS, Hamid O, et al. Atezolizumab, an anti-programmed death-ligand 1 antibody, in metastatic renal cell carcinoma: long-term safety, clinical activity, and immune correlates from a phase Ia study. J Clin Oncol 2016;34:833–42.
9. Sharma P, Hu-Lieskovan S, Wargo JA, Ribas A. Primary, adaptive, and acquired resistance to cancer immunotherapy. Cell 2017;168:707–23.
10. Rizvi NA, Hellmann MD, Snyder A, Kvistborg P, Makarov V, Havel JJ, et al. Cancer immunology. Mutational landscape determines sensitivity to PD-1 blockade in non-small cell lung cancer. Science 2015;348:124–8.
11. Van Allen EM, Miao D, Schilling B, Shukla SA, Blank C, Zimmer L, et al. Genomic correlates of response to CTLA-4 blockade in metastatic melanoma. Science 2015;350:207–11.
12. Zaretsky JM, Garcia-Diaz A, Shin DS, Escuin-Ordinas H, Hugo W, Hu-Lieskovan S, et al. Mutations associated with acquired resistance to PD-1 blockade in melanoma. N Engl J Med 2016;375:819–29.
13. Rodig SJ, Gusenleitner D, Jackson DG, Gjini E, Giobbie-Hurder A, Jin C, et al. MHC proteins confer differential sensitivity to CTLA-4 and PD-1 blockade in untreated metastatic melanoma. Sci Transl Med 2018;10:1–13.
14. Chowell D, Morris LGT, Grigg CM, Weber JK, Samstein RM, Makarov V, et al. Patient HLA class I genotype influences cancer response to checkpoint blockade immunotherapy. Science 2018;359:582–7.
15. McGranahan N, Rosenthal R, Hiley CT, Rowan AJ, Watkins TBK, Wilson GA, et al. Allele-specific HLA loss and immune escape in lung cancer evolution. Cell 2017;171:1259–71.
16. Gao J, Shi LZ, Zhao H, Chen J, Xiong L, He Q, et al. Loss of IFN-γ pathway genes in tumor cells as a mechanism of resistance to anti-CTLA-4 therapy. Cell 2016;167:397–404.
17. Manguso RT, Pope HW, Zimmer MD, Brown FD, Yates KB, Miller BC, et al. In vivo CRISPR screening identifies Ptpn2 as a cancer immunotherapy target. Nature 2017;547:413–8.
18. Patel SJ, Sanjana NE, Kishton RJ, Eidizadeh A, Vodnala SK, Cam M, et al. Identification of essential genes for cancer immunotherapy. Nature 2017;548:537–42.
19. Benci JL, Xu B, Qiu Y, Wu TJ, Dada H, Twyman-Saint Victor C, et al. Tumor interferon signaling regulates a multigenic resistance program to immune checkpoint blockade. Cell 2016;167:1540–54.

20. Sumimoto H, Imabayashi F, Iwata T, Kawakami Y. The BRAF-MAPK signaling pathway is essential for cancer-immune evasion in human melanoma cells. J Exp Med 2006;203:1651–6.

21. Spranger S, Bao R, Gajewski TF. Melanoma-intrinsic β-catenin signalling prevents anti-tumour immunity. Nature 2015;523:231–5.

22. Hugo W, Zaretsky JM, Sun L, Song C, Moreno BH, Hu-Lieskovan S, et al. Genomic and transcriptomic features of response to anti-PD-1 therapy in metastatic melanoma. Cell 2017;168:542.

23. Peng W, Chen JQ, Liu C, Malu S, Creasy C, Tetzlaff MT, et al. Loss of PTEN promotes resistance to T cell–mediated immunotherapy. Cancer Discov 2016;6:202–16.

24. Liu D, Schilling B, Liu D, Sucker A, Livingstone E, Jerby-Amon L, et al. Integrative molecular and clinical modeling of clinical outcomes to PD1 blockade in patients with metastatic melanoma. Nat Med 2019;25:1916–27.

25. Rosenthal R, Cadieux EL, Salgado R, Bakir MA, Moore DA, Hiley CT, et al. Neoantigen-directed immune escape in lung cancer evolution. Nature 2019;567:479–85.

26. Garrido F, Aptsiauri N, Doorduijn EM, Garcia Lora AM, van Hall T. The urgent need to recover MHC class I in cancers for effective immunotherapy. Curr Opin Immunol 2016;39:44–51.

27. Davis MM, Boniface JJ, Reich Z, Lyons D, Hampl J, Arden B, et al. Ligand recognition by alpha beta T cell receptors. Annu Rev Immunol 1998;16:523–44.

28. Verma V, Shrimali RK, Ahmad S, Dai W, Wang H, Lu S, et al. PD-1 blockade in subprimed CD8 cells induces dysfunctional PD-1CD38 cells and anti-PD-1 resistance. Nat Immunol 2019;20:1231–43.

29. van den Elsen PJ, Holling TM, Kuipers HF, van der Stoep N. Transcriptional regulation of antigen presentation. Curr Opin Immunol 2004;16:67–75.

30. Zhou F. Molecular mechanisms of IFN-γ to up-regulate MHC class I antigen processing and presentation. Int Rev Immunol 2009;28:239–60.

31. Parker BS, Rautela J, Hertzog PJ. Antitumour actions of interferons: implications for cancer therapy. Nat Rev Cancer 2016;16:131–44.

32. Benci JL, Johnson LR, Choa R, Xu Y, Qiu J, Zhou Z, et al. Opposing functions of interferon coordinate adaptive and innate immune responses to cancer immune checkpoint blockade. Cell 2019;178:933–48.

33. Pai C-CS, Huang JT, Lu X, Simons DM, Park C, Chang A, et al. Clonal deletion of tumor-specific T cells by interferon-γ confers therapeutic resistance to combination immune checkpoint blockade. Immunity 2019;50:477–92.

34. Burr ML, Sparbier CE, Chan Y-C, Williamson JC, Woods K, Beavis PA, et al. CMTM6 maintains the expression of PD-L1 and regulates antitumour immunity. Nature 2017;549:101–5.

35. Mezzadra R, Sun C, Jae LT, Gomez-Eerland R, de Vries E, Wu W, et al. Identification of CMTM6 and CMTM4 as PD-L1 protein regulators. Nature 2017;549:106–10.

36. Burr ML, Sparbier CE, Chan KL, Chan Y-C, Kersbergen A, Lam EYN, et al. An evolutionarily conserved function of polycomb silences the MHC class I antigen presentation pathway and enables immune evasion in cancer. Cancer Cell 2019;36:385–401.

37. Galluzzi L, Buqué A, Kepp O, Zitvogel L, Kroemer G. Immunological effects of conventional chemotherapy and targeted anticancer agents. Cancer Cell 2015;28:690–714.

38. Goel S, DeCristo MJ, Watt AC, BrinJones H, Sceneay J, Li BB, et al. CDK4/6 inhibition triggers anti-tumour immunity. Nature 2017;548:471–5.

39. Zhang J, Bu X, Wang H, Zhu Y, Geng Y, Nihira NT, et al. Cyclin D-CDK4 kinase destabilizes PD-L1 via cullin 3-SPOP to control cancer immune surveillance. Nature 2018;553:91–5.

40. Medina BD, Liu M, Vitiello GA, Seifert AM, Zeng S, Bowler T, et al. Oncogenic kinase inhibition limits Batf3-dependent dendritic cell development and antitumor immunity. J Exp Med 2019;216:1359–76.

41. Li W, Xu H, Xiao T, Cong L, Love MI, Zhang F, et al. MAGeCK enables robust identification of essential genes from genome-scale CRISPR/Cas9 knockout screens. Genome Biol 2014;15:554.

42. Wang B, Wang M, Zhang W, Xiao T, Chen C-H, Wu A, et al. Integrative analysis of pooled CRISPR genetic screens using MAGeCKFlute. Nat Protoc 2019;14:756–80.

43. Luo B, Cheung HW, Subramanian A, Sharifnia T, Okamoto M, Yang X, et al. Highly parallel identification of essential genes in cancer cells. Proc Natl Acad Sci U S A 2008;105:20380–5.

44. Zhou L, Mudianto T, Ma X, Riley R, Uppaluri R. Targeting EZH2 enhances antigen presentation, antitumor immunity, and circumvents anti-PD-1 resistance in head and neck cancer. Clin Cancer Res 2020;26:290–300.

45. Häcker H, Tseng P-H, Karin M. Expanding TRAF function: TRAF3 as a tri-faced immune regulator. Nat Rev Immunol 2011;11:457–68.

46. Jongsma MLM, Guarda G, Spaapen RM. The regulatory network behind MHC class I expression. Mol Immunol 2019;113:16–21.

47. Spel L, Nieuwenhuis J, Haarsma R, Stickel E, Bleijerveld OB, Altelaar M, et al. Nedd4-binding protein 1 and TNFAIP3-interacting protein 1 control MHC-1 display in neuroblastoma. Cancer Res 2018;78:6621–31.

48. Zarnegar BJ, Wang Y, Mahoney DJ, Dempsey PW, Cheung HH, He J, et al. Noncanonical NF-κB activation requires coordinated assembly of a regulatory complex of the adaptors cIAP1, cIAP2, TRAF2 and TRAF3 and the kinase NIK. Nat Immunol 2008;9:1371–8.

49. Vallabhapurapu S, Matsuzawa A, Zhang W, Tseng P-H, Keats JJ, Wang H, et al. Nonredundant and complementary functions of TRAF2 and TRAF3 in a ubiquitination cascade that activates NIK-dependent alternative NF-κB signaling. Nat Immunol 2008;9:1364–70.

50. Bista P, Zeng W, Ryan S, Bailly V, Browning JL, Lukashev ME. TRAF3 controls activation of the canonical and alternative NFκB by the lymphotoxin beta receptor. J Biol Chem 2010;285:12971–8.

51. Li S, Wan C, Zheng R, Fan J, Dong X, Meyer CA, et al. Cistrome-GO: a web server for functional enrichment analysis of transcription factor ChIP-seq peaks. Nucleic Acids Res 2019;47:W206–11.

52. Heinz S, Benner C, Spann N, Bertolino E, Lin YC, Laslo P, et al. Simple combinations of lineage-determining transcription factors prime cis-regulatory elements required for macrophage and B cell identities. Mol Cell 2010;38:576–89.

53. Mei S, Qin Q, Wu Q, Sun H, Zheng R, Zang C, et al. Cistrome Data Browser: a data portal for ChIP-Seq and chromatin accessibility data in human and mouse. Nucleic Acids Res 2017;45:D658–62.

54. Zheng R, Wan C, Mei S, Qin Q, Wu Q, Sun H, et al. Cistrome Data Browser: expanded datasets and new tools for gene regulatory analysis. Nucleic Acids Res 2019;47:D729–35.

55. Layer RM, Pedersen BS, DiSera T, Marth GT, Gertz J, Quinlan AR. GIGGLE: a search engine for large-scale integrated genome analysis. Nat Methods 2018;15:123–6.

56. Gilmore TD. Introduction to NF-κB: players, pathways, perspectives. Oncogene 2006;25:6680–4.

57. Vallabhapurapu S, Karin M. Regulation and function of NF-κB transcription factors in the immune system. Annu Rev Immunol 2009;27:693–733.

58. Sun S-C. The non-canonical NF-κB pathway in immunity and inflammation. Nat Rev Immunol 2017;17:545–58.

59. Hayden MS, Ghosh S. Shared principles in NF-κB signaling. Cell 2008;132:344–62.

60. Zhao B, Barrera LA, Ersing I, Willox B, Schmidt SCS, Greenfeld H, et al. The NF-κB genomic landscape in lymphoblastoid B cells. Cell Rep 2014;8:1595–606.

61. Link VM, Duttke SH, Chun HB, Holtman IR, Westin E, Hoeksema MA, et al. Analysis of genetically diverse macrophages reveals local and domain-wide mechanisms that control transcription factor binding and function. Cell 2018;173:1796–809.

62. Iannetti A, Ledoux AC, Tudhope SJ, Sellier H, Zhao B, Mowla S, et al. Regulation of p53 and Rb links the alternative NF-κB pathway to EZH2 expression and cell senescence. PLoS Genet 2014;10:e1004642.

63. Such L, Zhao F, Liu D, Thier B, Le-Trilling VTK, Sucker A, et al. Targeting the innate immunoreceptor RIG-I overcomes melanoma-intrinsic resistance to T cell immunotherapy. J Clin Invest 2020;130:4266–81.

64. Kalbasi A, Tariveranmoshabad M, Hakimi K, Kremer S, Campbell KM, Funes JM, et al. Uncoupling interferon signaling and antigen presentation to overcome immunotherapy resistance due to JAK1 loss in melanoma. Sci Transl Med 2020;12:eabb0152.

65. Lanier LL. NK cell recognition. Annu Rev Immunol 2005;23:225–74.

66. Jiang P, Gu S, Pan D, Fu J, Sahu A, Hu X, et al. Signatures of T cell dysfunction and exclusion predict cancer immunotherapy response. Nat Med 2018;24:1550–8.

67. Scheper W, Kelderman S, Fanchi LF, Linnemann C, Bendle G, de Rooij MAJ, et al. Low and variable tumor reactivity of the intra-tumoral TCR repertoire in human cancers. Nat Med 2019;25:89–94.

68. Font-Tello A, Kesten N, Xie Y, Taing L, Varešlija D, Young LS, et al. FiTAc-seq: fixed-tissue ChIP-seq for H3K27ac profiling and super-enhancer analysis of FFPE tissues. Nat Protoc 2020;15:2503–18.

69. Maude SL, Frey N, Shaw PA, Aplenc R, Barrett DM, Bunin NJ, et al. Chimeric antigen receptor T cells for sustained remissions in leuke-mia. N Engl J Med 2014;371:1507–17.

70. Gide TN, Quek C, Menzies AM, Tasker AT, Shang P, Holst J, et al. Distinct immune cell populations define response to anti-PD-1 mon-otherapy and anti-PD-1/anti-CTLA-4 combined therapy. Cancer Cell 2019;35:238–55.

71. Mariathasan S, Turley SJ, Nickles D, Castiglioni A, Yuen K, Wang Y, et al. TGFβ attenuates tumour response to PD-L1 blockade by con-tributing to exclusion of T cells. Nature 2018;554:544–8.

72. Vince JE, Wei-Lynn Wong W, Khan N, Feltham R, Chau D, Ahmed AU, et al. IAP antagonists target cIAP1 to induce TNFα-dependent apop-tosis. Cell 2007;131:682–93.

73. Varfolomeev E, Blankenship JW, Wayson SM, Fedorova AV, Kaya-gaki N, Garg P, et al. IAP antagonists induce autoubiquitination of c-IAPs, NF-κB activation, and TNFα-dependent apoptosis. Cell 2007;131:669–81.

74. Li B, Severson E, Pignon J-C, Zhao H, Li T, Novak J, et al. Compre-hensive analyses of tumor immunity: implications for cancer immu-notherapy. Genome Biol 2016;17:174.

75. Li T, Fan J, Wang B, Traugh N, Chen Q, Liu JS, et al. TIMER: a web server for comprehensive analysis of tumor-infiltrating immune cells. Cancer Res 2017;77:e108–10.

76. Gu SS, Wang X, Hu X, Jiang P, Li Z, Traugh N, et al. Clonal tracing reveals diverse patterns of response to immune checkpoint blockade. Genome Biol 2020;21:263.

77. Bertrand MJM, Milutinovic S, Dickson KM, Ho WC, Boudreault A, Durkin J, et al. cIAP1 and cIAP2 facilitate cancer cell survival by functioning as E3 ligases that promote RIP1 ubiquitination. Mol Cell 2008;30:689–700.

78. Beug ST, Beauregard CE, Healy C, Sanda T, St-Jean M, Chabot J, et al. Smac mimetics synergize with immune checkpoint inhibitors to promote tumour immunity against glioblastoma. Nat Commun 2017;8:14278.

79. Sun D, Wang J, Han Y, Dong X, Zheng R, Ge J, et al. TISCH: a com-prehensive web resource enabling interactive single-cell transcrip-tome visualization of tumor microenvironment. Nucleic Acids Res 2021;49:D1420–30.

80. Zhang H, Christensen CL, Dries R, Oser MG, Deng J, Diskin B, et al. CDK7 inhibition potentiates genome instability triggering anti-tumor immunity in small cell lung cancer. Cancer Cell 2020;37:37–54.

81. Hu-Lieskovan S, Mok S, Homet Moreno B, Tsoi J, Robert L, Goedert L, et al. Improved antitumor activity of immunotherapy with BRAF and MEK inhibitors in BRAF(V600E) melanoma. Sci Transl Med 2015;7:279ra41.

82. Topper MJ, Vaz M, Chiappinelli KB, DeStefano Shields CE, Niknafs N, Yen R-WC, et al. Epigenetic therapy ties MYC depletion to reversing immune evasion and treating lung cancer. Cell 2017;171:1284–300.

83. Aran D, Sirota M, Butte AJ. Systematic pan-cancer analysis of tumour purity. Nat Commun 2015;6:8971.

84. Li B, Li JZ. A general framework for analyzing tumor subclonality using SNP array and DNA sequencing data. Genome Biol 2014;15:473.

85. Xiao T, Li W, Wang X, Xu H, Yang J, Wu Q, et al. Estrogen-regulated feedback loop limits the efficacy of estrogen receptor-targeted breast cancer therapy. Proc Natl Acad Sci U S A 2018;115:7869–78.

86. Sanjana NE, Shalem O, Zhang F. Improved vectors and genome-wide libraries for CRISPR screening. Nat Methods 2014;11:783–4.

87. Shalem O, Sanjana NE, Hartenian E, Shi X, Scott DA, Mikkelson T, et al. Genome-scale CRISPR-Cas9 knockout screening in human cells. Science 2014;343:84–7.

88. Gu S, Sayad A, Chan G, Yang W, Lu Z, Virtanen C, et al. SHP2 is required for BCR-ABL1-induced hematologic neoplasia. Leukemia 2018;32:203–13.

89. Qin Q, Mei S, Wu Q, Sun H, Li L, Taing L, et al. ChiLin: a comprehen-sive ChIP-seq and DNase-seq quality control and analysis pipeline. BMC Bioinformatics 2016;17:404.

90. Li H, Durbin R. Fast and accurate short read alignment with Burrows-Wheeler transform. Bioinformatics 2009;25:1754–60.

91. Zhang Y, Liu T, Meyer CA, Eeckhoute J, Johnson DS, Bernstein BE, et al. Model-based analysis of ChIP-Seq (MACS). Genome Biol 2008; 9:R137.

92. Love MI, Huber W, Anders S. Moderated estimation of fold change and dispersion for RNA-seq data with DESeq2. Genome Biol 2014;15:550.

AAGR American Association
for Cancer Research

CANCER DISCOVERY

Therapeutically Increasing MHC-I Expression Potentiates Immune Checkpoint Blockade

Shengqing Stan Gu, Wubing Zhang, Xiaoqing Wang, et al.

Cancer Discov Published OnlineFirst February 15, 2021.

Updated version	Access the most recent version of this article at: doi:10.1158/2159-8290.CD-20-0812
Supplementary Material	Access the most recent supplemental material at: http://cancerdiscovery.aacrjournals.org/content/suppl/2021/01/16/2159-8290.CD-20-0812.DC1

E-mail alerts	Sign up to receive free email-alerts related to this article or journal.
Reprints and Subscriptions	To order reprints of this article or to subscribe to the journal, contact the AACR Publications Department at pubs@aacr.org.
Permissions	To request permission to re-use all or part of this article, use this link http://cancerdiscovery.aacrjournals.org/content/early/2021/05/19/2159-8290.CD-20-0812. Click on "Request Permissions" which will take you to the Copyright Clearance Center's (CCC) Rightslink site.